TO THE GRADUATE COUNCIL:

I am submitting herewith a dissertation written by Raj K. Kaul entitled "Compatibility Problems Generated in Graphite Fiber--Metal Matrix Composites." I have examined the final copy of this dissertation for form and content and recommend that it be accepted in partial fulfillment of the requirements for the degree of Doctor of Philosophy with a major in Engineering Science.

Maurice A. Wright, Major Professor

We have read this dissertation
and recommend its acceptance:

Accepted for the Council:

The Graduate School

COMPATIBILITY PROBLEMS GENERATED IN GRAPHITE FIBER -- METAL MATRIX COMPOSITES

A Dissertation

Presented for the

Doctor of Philosophy

Degree

The University of Tennessee, Knoxville

Raj K. Kaul

August 1984

ACKNOWLEDGMENTS

The author wishes to express his sincere appreciation to Dr. M. A. Wright, Thesis Committee Chairman and Major Professor, for his continual assistance, support, and technical guidance throughout the course of this study.

A special note of thanks to Mr. M. K. White and Mr. M. K. Bhat for their cooperation, help, and discussion throughout this research. Thanks are also extended to the Library Staff at The University of Tennessee Space Institute for their assistance in obtaining copies of technical reports and papers necessary as reference material for this research. Appreciation is also expressed to Mrs. L. W. Hershman for her dedicated assistance in typing this dissertation.

The author's deepest gratitude is extended to his parents and S. L. Witt, whose encouragement, patience and support of his endeavors was instrumental in the completion of this dissertation.

ABSTRACT

The matrix of graphite fiber reinforced resin composites limits their useful temperature of application to a maximum of about 300° C. Efforts have been made to increase the usable temperature of graphite fiber composites by incorporating the fibers into metal matrices. The present study describes the work in this area and covers aspects such as chemical compatibility, composite fabrication technology and mechanical properties.

The single graphite fibers coated with nickel have been shown to undergo structural recrystallization. Techniques have been developed to stop the structural recrystallization by coating the fibers with barrier coatings such as pyrolytic graphite.

A method of composite fabrication has been developed. Graphite-7075Al alloy, graphite-Pb, 2 percent Sn alloy, and graphite-Zn, 2 percent Sn alloy composites have been fabricated by liquid metal infiltration of nickel-coated graphite fibers. Nickel coating acts as a coupling agent to improve the wetting of graphite fibers by molten metals or alloys. A heat-treatment method has been developed to improve the tensile strength of graphite-Al composite. Typical mechanical and physical properties of these composites are presented, and potential applications for these materials are explored.

TABLE OF CONTENTS

CHAPTER		PAGE
I.	INTRODUCTION	1
II.	LITERATURE REVIEW	4
	Nickel-Graphite Recrystallization	9
	Barrier Coatings	12
	Aluminum-Graphite Composites	16
	Wetting	16
	Lead-Graphite and Zinc-Graphite	19
III.	EXPERIMENTAL TECHNIQUE	22
	Nickel-Graphite	23
	Aluminum-Graphite, Zinc-Graphite, and Lead-Graphite	26
	Mechanical Property Measurements	28
	Physical Property Determination	29
	Metallographic Observations	31
IV.	EXPERIMENTAL RESULTS	32
	Nickel-Graphite Fiber System	32
	Composite Mechanical Properties	34
	Composite Densities	35
	Metallographic Observations	36
V.	DISCUSSION	38
	Nickel-Graphite System	38
	Composite Fabrication	40
	Aluminum-Graphite	41

CHAPTER PAGE

V. (Continued)

Zinc-Graphite and Lead-Graphite Composite 42

Calculation of Nickel and Fiber Content 42

Void Fraction 45

Mechanical Properties 46

Effect of Voids on Strength 50

Effect of Fiber Orientation on Strength 53

Graphite-Aluminum Composite 55

Effect of Directional Solidification 56

Statistical Comparison of As-Cast and Directionally Solidified Composite 58

VI. CONCLUSIONS 60

VII. RECOMMENDATIONS 61

LIST OF REFERENCES 62

APPENDIX 67

VITA 127

LIST OF TABLES

TABLE		PAGE
I.	Comparison of Some of the Properties and the Cost of Various Fibers	68
II.	Properties of Commercially Available Graphite Fibers	69
III.	Some of the Advantages and Disadvantages of a Metal Matrix Compared with a Resin Matrix	70
IV.	Mechanical and Physical Properties of As-Cast Graphite Metal Composites	71
V.	Percent Voids in Composite	73
VI.	Effect of Zone Travel Rate on Strength of Fortifil 5 Graphite-Al_3Ni-Al Composite	74
VII.	Rank Test	75
VIII.	Chi-Square Distribution	76

LIST OF FIGURES

FIGURE		PAGE
1.	Graphite crystal lattice	77
2.	Schematic of observed carbon fiber structures	78
3.	Schematic diagram of onion-skin model for graphite fibers .	79
4.	The activity of carbon (standard state = graphite) for several metal-carbide systems as a function of temperature	80
5.	Effect of isothermal exposure of graphite fibers, in vacuum, on the strength (a) uncoated graphite fibers, and (b) nickel-coated graphite fibers	81
6.	The model system -- fiber/layer	82
7.	Wetting of graphite by melts	83
8.	Nickel-coated graphite fibers, 1815X	84
9.	Set-up for heating nickel-coated graphite fibers	85
10.	Apparatus to coat pyrolytic carbon on fiber tows	86
11.	Nickel-coated Fortifil 5 fibers obtained from Great Lakes Carbon Corp., 2200X	87
12.	Experimental set-up, to fabricate the composite rods	88
13.	Graphite mold used to fabricate the composites of rectangular shape	89
14.	The structural shapes in which the composites can be fabricated	90
15.	Zone melting unit	91

FIGURE PAGE

16. Specimen mount and the graphite-Al composite specimens for directional solidification 92

17. Instrumented test specimen mounted in the tensile machine . 93

18. Fortifil 5 graphite fibers Ni-coated and heat-treated at 850° C for two hours 94

19. Fortifil 5 PAN-based fibers partially recrystallized by nickel after heating for one hour at 1,000° C 95

20. Fortifil 5 PAN-based graphite fibers fully recrystallized by nickel after one hour at 1,100° C 96

21. Pitch-based graphite fibers fully recrystallized by nickel after one hour at 1,100° C, 2500X 97

22. Strength of nickel-coated Fortifil 5 graphite fibers after heating for one hour at various temperatures 98

23. Fortifil 5 graphite fibers oxidized 99

24. Fortifil 5 PAN-based graphite fibers air-oxidized for one hour at 1,100° C; nickel-plated, and heated one hour at 1,100° C, 2500X 102

25. Fortifil 5 PAN-based graphite fiber sputter-coated with carbon, nickel-plated and heated for one hour at 1,100° C, 2500X 103

26. Fortifil 5 fiber Pyrdytic-carbon-coated, nickel-coated and heated at 1,100° C for one hour, 3000X 104

27. Fortifil 5 PAN-based graphite fibers with carbonized epoxy resin-coating and nickel-plating after one hour, 1,100° C heat treatment, 2500X 105

FIGURE PAGE

28. Mono-carbon fiber, coated with pyrolytic carbon (HT 2,700° C, one hour) obtained from AVCO, nickel-coated and heated at 1,100° C for 24 hours, 3000X 106

29. Strength of nickel-coated-AVCO graphite fibers (pyrolytic-coated, heat-treated at 2,700° C for one hour) after heating for two hours at various temperatures . 107

30. Tensile strength vs. volume percent of fibers plot of various composites (as-cast and after-directional solidification in the case of Al-graphite) 108

31. Tensile modulus vs. volume percent of fibers plot of various composites (as-cast and after-directional solidification in the case of Al-graphite) 109

32. Transverse micrographs of Fortifil 5 and Fortifil 3 graphite fiber composites 110

33. SEM photograph of the fractured surface of Fortifil 5-7075Al composite (as-cast), 400X 113

34. The crack propagation through brittle Al_3Ni matrix in as-cast Fortifil 5-7075Al composite, 236X 114

35. Longitudinal micrographs of Fortifil 5-7075Al composites . . 115

36. SEM photograph of fractured surface of Fortifil 5-7075Al composite directionally solidified at 10"/hour rate, 1000X 118

37. Longitudinal micrograph of the directionally solidified Fortifil 5-7075Al composite. The solidification rate being 2.5 inches per hour, 236X 119

FIGURE PAGE

38. Fortifil 5 graphite fibers Ni-coated, heated at 1,100° C for one hour and again Ni-coated and heat-treated at 1,100° C for one hour in vacuum, 1815X 120

39. Al-Ni equilibrium diagram 121

40. Ni-Zn equilibrium diagram 122

41. Ni-Pb equilibrium diagram 123

42. Model of local high-void density volume of bundle fracture . 124

43. Longitudinal micrograph of Fortifil 5 graphite fibers-7075Al composite after directional solidification. Rate of zone passing 14"/hour, 236X 125

44. Fiber orientation. Schematic representation of a composite containing aligned fibers oriented at an angle ϕ to the tensile axis 126

CHAPTER I

INTRODUCTION

The composite materials technology is considered as one of the ancient materials technologies. Early civilizations, which used laminated bows for extra strength and mixtures of straw (for reinforcing fiber) and mud (matrix) for building bricks, are cited as some of the first users of composite materials. Although these ancient materials can be broadly classed as types of composite materials, the modern science of composite materials began relatively recently. The reason for the recent increased interest has been the development of high performance fibers which make it technically feasible to produce composite materials with vastly improved mechnical properties. The high specific strength and modulus properties of fibrous composite materials have resulted in much interest in their use for applications requiring high strength at low weight, particularly in the design of aerospace structures.

Different people have given different definitions for the composites. Here are some precise definitions:

1. Composites are compound materials which differ from alloys by the fact that the individual components retain their characteristics but are so incorporated into the composite as to take advantage only of their attributes and not of their shortcomings in order to obtain an improved material [1].

2. Composites are multifunctional systems that provide characteristics not obtainable from any discrete material. They are cohesive structures made by physically combining two or more compatible materials, differing in composition and characteristics and, sometimes, in form. [2].

From the above definitions, it clearly results that what has to be achieved during the design and the fabrication of a composite material is the incorporation into its structure of a synergistic effect so as to be able to obtain a new material possessing superior properties to the individual components. The basis for filamentary composites is that the strength and modulus of brittle materials are traded off for a measure of impact strength.

Carbon and graphite fibers are of great interest as reinforcements in metal-matrix composites because of their strength and stiffness, low density, and potential for large-scale production at low cost. The comparison of these properties of graphite fiber with other fibers is shown in Table I.* Graphite has a major cost and density advantage over boron and modulus, and density advantage over glass fibers. Additionally, graphite fibers retain their properties to very high temperatures, at which glass is softened and organic fibers, such as PRD-49, are unusable. Pitch base fibers have a substantially lower raw materials cost and, possibly, a lower processing cost. The process has yet to be commercialized. This process has the possibility of producing fibers in the $1/lb. to $3/lb. range.

---

*All Tables appear in Appendix.

Graphite fibers are attractive as reinforcements for metals. However, two major problems are encountered:

1. Graphite fibers are incompatible with many metals at elevated temperatures, since they tend to react to form a metal carbide or they recrystallize. When either of these two phenomena occur, the strength and modulus values decrease dramatically.
2. Graphite fibers are difficult to wet by liquid metals; thus, liquid metal infiltration techniques are difficult to apply.

The lack of fiber wettability may be alleviated by the use of fiber coatings with sufficiently high surface energy to produce wetting by molten metals. Nickel is an advantageous choice because of its ease of deposition and relatively high melting temperature. In the present investigation, nickel was used as a wetting agent in the Al-graphite, Pb-graphite, and Zn-graphite systems. Barrier coatings may be used to prevent reaction and dissolution of the graphite fibers with the matrices or wetting layer (nickel) by limiting the transport of carbon. Vitreous carbon and pyrolytic graphite coatings were investigated in the present study.

CHAPTER II

LITERATURE REVIEW

Commercial high-performance graphite fibers have been produced from either rayon or polyacrylonitrile (PAN) precursors. The processing of these precursors to graphite fibers is the subject of several patents which vary in detail. In general, the PAN precursor is stretched approximately 80 percent prior to, or during, stabilization. The stabilization cycle involves heating the fiber at 220° C for 24 hours in air; the fiber is under axial tension and no axial shrinkage is permitted at this stage. Carbonization consisting of slowly heating the fiber in an inert atmosphere to 1,000° C follows. After carbonization, the fibers are graphitized by raising the temperature to graphitization temperatures, in the range of 1,000° C to 2,500° C [3].

The graphitic form of carbon has a hexagonal crystal structure similar to that illustrated in Figure 1.* In the hexagonal graphite lattice, each carbon atom has four valence electrons. Three of these form tight covalent bonds with neighboring atoms; the fourth is more loosely bound. Since each carbon atom is surrounded by three neighbors at equal distances, and in a single plane, a hexagonal ring structure results. The layers formed by these rings are bonded together by much weaker Van der Waal forces. Adjacent atoms in any layer are closer (1.42° A) than the spacing (3.25° A) between layers. This atomic

---

*All Figures appear in Appendix.

configuration results in extreme anisotropy in the crystal structure [4]. Graphite is unique among engineering materials in that parallel to the basal planes, its specific modulus (modulus/weight ratio) is the largest known, while very low values of the same property are recorded normal to these planes.

The chemical stability of graphite fibers depends upon the orientation and ordering of the crystallite structure at the fiber surface [4]. As the extent of axial-preferred orientation, and the average crystallite size, increases and interplaner spacing decreases, the stability of the fiber is improved. These same conditions also result in higher strength and modulus. Fiber structural studies have shown that highly graphitized (high modulus) rayon-based and PAN-based fibers of about 8μm diameter have a duplex structure, Figure 2, consisting of an outer sheath (about 1.5μm thick) of concentrically-aligned layers with higher axial alignment and lower crystallite size than the fiber average and a core of layers in a radial configuration with lower axial alignment and larger-than-average crystallite size [3,5,6]. Low-energy, highly stable, basal planes are presented at the fiber surface, resulting in high resistance to dissolution and chemical reaction. In contrast, low-modulus fibers, produced at lower graphitization temperatures, are essentially homogeneous through the cross-section having more or less random basal plane orientations. Many high-energy basal-plane edges are, therefore, present at the fiber surface, resulting in greater chemical activity than for the higher-modulus fibers.

When PAN-based graphite fibers of circular cross-section are viewed under polarized light, they display extinction crosses, indicating a circular symmetry of structure. This observation led to the development of the onion-skin model [5]. This model proposed that in such fibers, the basal planes tend to be parallel to the fiber circumference with a corresponding radial orientation of the 'C' direction, Figure 3(a). Dog-bone section fibers have also been examined under polarized light and a structure similar to the onion-skin model proposed [5]. However, because of the geometry, the basal planes tend to be preferentially aligned in the longitudinal direction of the fiber cross-section, Figure 3(b). X-ray and electron diffraction studies have confirmed that in graphite fibers, a preferential alignment of the basal planes parallel to the fiber axis exists. The length of time the fiber is held at stabilization temperatures and the subsequent heating rate during carbonization were shown to affect the radial orientation of both round and dog-bone sectioned fibers [5]. It is important to know the degree of basal-plane orientation along the length of a graphite fiber, as this will determine fiber strength and modulus. Further, the surface energy of graphite fibers determines their tendency to be wet by the matrix and the bonding characteristics in a composite. Basal planes exhibit a very low-surface energy, resulting in a low degree of adhesion and wetting of these fibers by matrix materials. For PAN-based fibers, the processing required to produce higher modulus also results in an increased preferential alignment of basal-plane surfaces parallel to the fiber surface so that,

in general, the higher the modulus, the lower the adhesion between fibers and matrix. Consequently, graphite fiber-epoxy composites made from high-modulus fibers display low shear strengths. Failure usually occurs at the epoxy-fiber interface [7].

A wide range of properties is available in graphite fibers dependent upon the organic precursor and processing conditions employed. The typical properties of graphite fibers are given in Table II. Tensile strengths may be obtained between 150 and 450 ksi and tensile moduli between 25 and 75 msi. In general, a greater degree of graphitization results in a fiber of higher strength, modulus and density.

Composites consisting of a polymer such as epoxy reinforced with graphite fibers are employed for applications where a high-strength or modulus-to-weight ratio is required. Application areas include aircraft structures, re-entry vehicles, space vehicles and marine deep-submergence pressure vessels. Much literature exists in which are described the properties and application of these polymer-matrix systems. It should be noted, however, that the resin matrix of these composites limits their use to relatively lower temperatures. Efforts have, therefore, been made to increase the usable temperature of graphite fiber composites by incorporating the fibers into metal matrices. In addition, metals have a number of other advantages over thermosetting resins as a matrix for reinforcement. For instance, their higher thermal conductivity permits better heat removal from components and they have better resistance to ultraviolet radiation and moisture. A complete listing of these advantages is included in Table III.

The preparation of metal-graphite composites has been attempted using methods quite familiar to materials-fabrication specialists; these include powder metallurgy, diffusion bonding, and liquid metal infiltration. Powder metallurgy and diffusion bonding are processes that are not readily adaptable to the fabrication of metal-graphite composites because they do not permit the matrix metals to penetrate all of the interstices of the individual small (7-8μm) fibrils that make up the commercial fiber tows. Conversely, the metal-infiltration technique is potentially capable of insuring that the metal penetrates the interstices of the fibers and is cost-effective. Unfortunately, as stated before, most of the molten metals either do not wet the graphite fibers, or they form property-reducing carbides with the fiber.

A large proportion of the experimental work concerned with reinforcing metals with graphite fibers has involved experiments that dealt with the compatibility problem. Aluminum, magnesium, nickel and cobalt have been found to be fairly compatibile with graphite fibers at temperatures less than 800° C. Metal-graphite couples have been divided into two general groups depending on whether the metals form carbides at high temperatures [8]. Examples of carbide formers are aluminum, titanium, molybdenum and chromium. Among the metals that do not readily form carbides, are nickel, cobalt, copper, zinc and lead. Both groups may be expected to damage the graphite fibers at some temperature, either by producing brittle carbide surface layers or by dissolving the fiber. The tendency towards carbide formation can be estimated from a plot of log carbon activity versus reciprocal temperature [9],

Figure 4. This thermodynamic information is not, in itself, adequate to estimate the extent of the property degradation since it gives no indication of the rate of carbide formation which depends on the diffusion characteristics of carbon through the metallic and carbide phases, as well as on the form and continuity of the carbides.

Metals such as aluminum and magnesium exhibit appreciable carbide formation only at temperatures well above their usable limits. Therefore, carbide formation poses a problem in these systems only in regard to fabrication, which is usually at substantially higher temperatures. The problem of graphite fiber dissolution in some non-carbide forming matrices, such as nickel, is more acute since it occurs both at desirable use temperatures and, to a greater extent, at fabrication temperatures. However, both types of incompatibilities may be alleviated (at least, in part) by modifications to the composite systems and/or the fabrication procedures. These modifications are the subject of the present investigation.

Nickel-Graphite Recrystallization

As stated in the previous section, a fiber coating, such as nickel, may be used as a wetting or coupling agent to permit infiltration of graphite fibers by molten metals. However, at temperatures above about 800° C, either during fabrication or subsequent service, the graphite fibers have been found to undergo a dissolution-reprecipitation type of degradation in a nickel matrix that may totally destroy the reinforcing effect of the fibers. The same phenomenon also occurs in some other matrices, such as cobalt [12]. However, very little

investigation has been made of those matrices compared to nickel.

At elevated temperatures, mass transport of a diffusing species takes place due to gradients of chemical potential. Any form of material transport which is accompanied by morphological and mechanical property degradation of the fibers is of importance, since the mechanical properties of the composite ultimately depend upon physical property retention by the reinforcing phase.

Unfortunately, graphite-nickel composites have been shown to be vulnerable to both oxidation [10,11] and structural degradation of the fibers [12-15] at elevated temperatures so that complete loss of the favorable mechanical properties can occur. The mechanism of the oxidation process involves the highly active monoatomic form in which the oxygen is present at the coated metal-fiber interface. The structual degradation involves fiber restructuring, which occurs at high temperatures in the presence of a nickel matrix. The process, called "recrystallization," involves a change from characteristic oriented fiber structure to the coarse, randomly oriented graphite crystals. The results of Jackson and Marjoram [12] indicate that the recrystallization process becomes rapid over a narrow temperature range, leading to strength degradation as shown in Figure 5(b). Experimental evidence supporting this mechanism began with identical heat treatments applied to both nickel-coated and uncoated fibers [12]. Since there was no degradation in the strength of uncoated fibers, but a large degradation of coated fibers, the nickel coating was obviously a vital participant in the degradation process.

The recrystallization temperature was found to vary considerably depending upon the type of fiber, the purity of the matrix, and the environment used in the heating experiments. Jackson and Marjoram [12] found that high-modulus PAN-based fibers coated with electrolytically-deposited nickel recrystallized rapidly at about 1,000° C in a vacuum. Warren, Anderson and Carlson [15] determined recrystallization temperatures of about 1,000° C for Courtaulds HM fibers and 1,200°-1,230° C for Modmor I fibers in high purity flowing argon. Sarian and Warren, et al., [13,15], found that nickel-coated rayon-based HM fibers did not recrystallize during prolonged annealing at 1,200° C, but did so at 1,250°-1,270° C.

Barclay and Bonfield [16] noted that metal spheroids were formed on the surface of nickel-coated fibers when they were heated at 1,000° C. These spread out, on continued heating at 1,100° C, to reform a continuous coating. The degradation in strength of the fibers was found to correlate approximately with the formation of this continuous coating. These authors postulated that carbon/carbon bond separation was the rate-controlling process for the degradation in strength of the fibers since the activation energy for the re-wetting process agreed approximately with carbon/carbon bond energy. They suggested that Jackson and Marjoram's [12] results were influenced by the presence of impurities, such as sulphur, in the electro-deposited nickel; these impurities could lower the effective carbon/carbon bond energy by forming an alternative bond (such as carbon/sulphur) and so reduce the temperature at which strength

degradation occurs. Kistler and Niesz [17] also suggested that Jackson's results may have been influenced by impurities (such as oxygen and hydrogen) in the nickel coating; it was thought that such impurities would have been eliminated by the outgassing heat treatment given to their electroless nickel-coated Thornel 50 fibers. They observed no sign of large-scale degradation in fiber morphology after 100 hours at 1,200° C. Some of the conflicting observations could have arisen from differences in (a) the type of fiber, (b) the purity of the nickel coating, and (c) the experimental conditions.

While both oxidation and restructuring of graphite fibers at high temperatures in the presence of the nickel matrix present formidable problems, various approaches may be foreseen towards overcoming them. Both may be lessened by fiber diffusion-barrier coatings and by matrix alloying [14]. As indicated by Shiota and Watanabe [14], a slight oxidative treatment to the fiber has some effect on increasing fiber stability.

Barrier Coatings

The most important criteria that must be satisfied if a barrier coating is to protect the fiber from reaction with a matrix are: (a) intimate contact with the fiber; (b) wettability by the matrix; (c) high-temperature strength; (d) compatible coefficient of linear expansion with both the filament and the matrix; (e) thermal and metallurgical stability; (f) continuity and thickness uniformity; and (g) availability. Oxides, borides, nitrides, silicides, carbides, and several intermetallic compunds possess most of the properties

mentioned and could be used as protective coatings. Rashid, et al., have successfully coated the graphite fibers with carbides (Nb_2C and Ta_2C) [18]. Zabolotskii, et al., coated the fibers with zirconium nitride and titanium carbide [19]. They observed that the zirconium nitride coating failed to prevent graphite fibers from reacting with nickel while the titanium carbide coating reduced, even at high temperatures, the strength loss experienced by graphite fibers by decreasing the rate of dissolution of the material of the fibers in nickel and, thereby, slowing down the fiber recrystallization process.

In order to prevent initiation of composite fracture in a brittle barrier coating and to avoid overdilution of the fiber content in the composite, it is necessary to minimize the coating thickness. A model, developed by Shorshorov, et al., allows the critical thickness of the layer to be determined. This is illustrated in Figure 6 [20]. The model depends on the Weibull theory, which assumes that there is an equal probability of finding a strength-reducing flaw in any volume. Weibull has shown [21] that the strength of brittle materials is affected by their volume according to the equation

$$\sigma_1/\sigma_2 = (v_2/v_1)^{1/\beta} \qquad (2\text{-}1)$$

where σ_1 and σ_2 are the average tensile strengths of a brittle material, having volumes v_1 and v_2, respectively, and β is a Weibull coefficient, which shows the strength distribution of the material.

This implies that if the length of the layer is unity, the tensile strength of the brittle layer is increased by a decrease in its area

(which is the factor of coating thickness). Hence, Equation 2-1 can be written as

$$\sigma_{\ell 1}/\sigma_{\ell 2} = (A_{\ell 2}/A_{\ell 1})^{1/\beta} \qquad (2\text{-}2)$$

where $\sigma_{\ell 1}$ and $\sigma_{\ell 2}$ are the average tensile strengths of brittle layers having cross-sectional areas of $A_{\ell 1}$ and $A_{\ell 2}$, respectively, and β is a Weibull coefficient of the tensile strength distribution of the layer. Now let the layer thickness be such that the average strain to failure $\varepsilon_{u\ell}$ of the layer be equal to the average strain to failure ε_{uf} of the fiber

$$\varepsilon_{uf} = \varepsilon_{u\ell} \qquad (2\text{-}3)$$

Since the brittle layer contains flaws, its failure strain decreases with thickness. The criterion of failure strain of the layer equal to the failure strain of the fiber defines the critical layer thickness beyond which the presence of the layer is detrimental to the fiber. Equation 2-3 is transformed into the following by Hooke's law

$$\sigma_{uf}/E_f = \sigma_{u\ell}/E_\ell \qquad (2\text{-}4)$$

where E_f and E_ℓ are the Young's moduli of the fiber and the layer, respectively; σ_{uf} is the average (statistical) tensile strength of the fiber, and $\sigma_{u\ell}$ is the average (statistical) tensile strength of a layer of given thickness (critical thickness, for the present).

Assume $\sigma_{u\ell} = \sigma_{\ell 2}$; $\sigma_{\ell 1} = \sigma_{u\ell 1}$; $A_\ell^* = A_{\ell 2}$ and $A_\ell = A_{\ell 1}$.

Then, combining Equations 2-1 and 2-2 gives

$$A_\ell^* = A_\ell(E_f\sigma_{u\ell 1}/E_\ell\sigma_{uf})^\beta \qquad (2\text{-}5)$$

where A_ℓ^* is the critical cross-sectional area of the layer of critical thickness.

Let d be the diameter of the fiber

$$A_\ell^* = \pi/4\left[(d + 2t_\ell^*)^2 - d^2\right]$$

and

$$A_\ell = \pi/4\left[(d + 2t_\ell)^2 - d^2\right]$$

Therefore, modification of Equation 2-5 gives

$$t_\ell^* = \left[(d/2)^2 + t_\ell(d + t_\ell)(E_f\sigma_{u\ell 1}/E_\ell\sigma_{uf})^\beta\right]^{1/2} - d/2 \qquad (2\text{-}6)$$

where t_ℓ is the known value of the thickness of the layer for which $\sigma_{u\ell 1}$ is known, t_ℓ^* is the critical thickness of the layer.

Let $t_\ell = d$ be the diameter of the fiber for which $\sigma_{u\ell 1} = \sigma_{u\ell d}$

$$t_\ell^* = \left[(d/2)^2 + 2d^2(E_f\sigma_{u\ell d}/E_\ell\sigma_{uf})^\beta\right]^{1/2} - d/2$$

$$t_\ell^* = d\left[(1/4 + 2(E_f\sigma_{u\ell d}/E_\ell\sigma_{uf})^\beta)^{1/2} - 1/2\right]$$

The derived equation for the calculation of the critical thickness of the layer shows that it is proportional to the diameter of the fiber and is affected by the tensile strength and Young's moduli of the fiber and the layer.

Aluminum-Graphite Composites

Aluminum is an attractive matrix for reinforcement with graphite fibers for structural applications because of its low density and good corrosion resistance.

Production of aluminum-graphite composites was first attempted in 1961, when Koppenaal and Parikh used chopped graphite fibers mixed with an aluminum-copper alloy powder in a hot extrusion process [22]. This research was discontinued because of the low strength of the graphite fibers available at that time.

In a series of investigations of aluminum-graphite composites, Sara, et al., investigated the use of external pressure to force molten aluminum into graphite-fiber bundles, but the bundles were not infiltrated [23]. It was concluded from this work that infiltration could not be accomplished by using pressure alone, and that improvement of the wetting of graphite by aluminum was necessary in order to achieve infiltration.

Wetting

Wetting is the ability of a liquid metal to flow over the graphite fiber, i.e., that condition when the surface energy of the graphite fiber exceeds that of the liquid metal. The surface-free energy γ of the molten metal can be expressed as a function of the contact angle θ of the liquid with the graphite fiber [24]. The relation is illustrated below: the balance of surface energies is shown schematically in Figure 7, and is given by the equation

$$\gamma_s = \gamma_{s\ell} + \gamma_\ell \cos(\theta)$$

where s and ℓ stand for solid and liquid, respectively. Figure 7a illustrates the experimental observation obtained when a liquid metal drop does not wet the surface on which it is placed; and Figure 7b illustrates the situation when wetting has occurred. Therefore, some wetting has occurred when the contact angle is observed to be less than 90 degrees.

Sara observed that molten aluminum at elevated temperatures promoted wetting by forming carbide (Al_4C_3) but caused severe degradation of the fiber strength. He also investigated several techniques for cladding graphite fibers to prevent chemical interaction with aluminum and promote wetting. He coated fibers with TiC by CVD (Chemical Vapor Deposition) process. Satisfactory coatings were obtained, but tensile tests of the fibers showed them to be severely degraded by the coating process. Sara also studied the use of tantalum and nickel as coupling agents. The tantalum coating was found to have potential as a coupling agent. The nickel coating reacted with the aluminum to form significant quantities of Al_3Ni, which is a brittle phase, reducing the strength of the composite.

Schmidt and Hellman developed a method for plating aluminum on substrates by using aluminum hydride as a source material and contacting it with a decomposition catalyst [25]. Although the yarn appeared to be uniformly covered with aluminum, the bond was very poor and the coating could be wiped off.

Lalacona developed a process combining Thornel-50 fibers coated with electroless nickel and 1100 aluminum foil and hot-pressed at 1,000° F to a composite [26]. There is some doubt that this process can be used for production of composites with a high volume fraction of

graphite fibers, because of inability of the foil metal to penetrate the fibers.

Davis and Bradstreet obtained aluminum-electroplated Thornel fibers and consolidated them to produce composites by diffusion bonding [27]. The fiber pull-out during testing indicated an unsatisfactory bond between the fiber and plating.

DeLamotte and co-workers reported the fabrication of a continuously cast aluminum-graphite composite [28]. In this method, a nickel-coated graphite fiber tow is drawn through a die located at the bottom of a crucible that contains the aluminum melt. The liquid metal wets and permeates the tow and solidifies, producing a continuous wire. As the volume fraction of the fiber increases, the strength of the composite falls because of the increase in proportion of the Al_3Ni phase in the matrix of the composite.

Pepper, et al., produced aluminum-graphite composites by the sodium process [29]. The process consists of sequentially immersing graphite fibers in three molten metal baths. The first bath is sodium, the second is tin, and the third is aluminum or an aluminum alloy. They observed that Rayon-base graphite fibers, and some PAN-base fibers, exhibit no appreciable strength loss as a result of the processing, whereas, some PAN-base fibers are significantly degraded.

At the Aerospace Corporation, Kendall, et al., co-vapor deposited titanium and boron on graphite fibers immediately before the molten infiltration process [30]. The coating improved the wetting of the graphite fibers by molten aluminum. This process requires elaborate reaction chambers and close control over experimental conditions.

As reported by Sara, nickel used as a coupling agent forms intermetallic Al_3Ni with aluminum. It has been observed that many intermetallics grow naturally in filamentary form or can be induced to do so by unidirectional solidification of an appropriate eutectic. Hertzberg and associates have formed whiskers of Al_3Ni in this manner [31]. There has been much work reported on unidirectional solidification of Al-Ni eutectic alloys. Hertzberg, et al., observed that the presence of approximately 10 volume percent Al_3Ni whiskers aligned parallel to the stress axis resulted in a greater than threefold increase in tensile strength as compared to that exhibited by an as-cast Al-Ni eutectic alloy [32]. Verhoeven, et al., showed that the large temperature gradients may prove advantageous in enhancing regular coupled growth (eutectic type) in off-eutectic compositions [33].

Lead-Graphite and Zinc-Graphite

Lead and lead alloys are of great importance in the chemical, battery, building, and bearing industries because of their high resistance to corrosion in many chemical environments, acoustical damping, and excellent anti-frictional properties. However, the low strength of lead and its alloys imposes severe limitations on their use. One solution to this problem appears to be through graphite fiber strengthening. A major cause of failure in lead-acid batteries is buckling of the lead plates because of low stiffness.

The formation of lead-graphite composites by electroplating lead onto a 1,000 -- 2,500 filament graphite tow and hot-compacting has been described by Baker, et al. [34]. Molten lead does not spontaneously wet the graphite fibers, as was observed by Goddard, et al. [35]. They developed two processes for the preparation of lead-graphite composites, both of which produced good infiltration of multifilament fiber bundles with lead. First, is the sodium process in which the fiber bundle is passed through molten sodium, which has the ability to wet and infiltrate the bundle; and then through the molten lead, to fabricate the composite. This process was found to contaminate the lead matrix. Second, is the chemical vapor codeposition of titanium and boron on graphite fiber bundles, the coating treatment making graphite fibers wettable by molten lead.

The major structural use of zinc is in Zn-alloy die casting in automotive, home appliance, and machinery products. The most severe limitation in the use of Zn-alloys is the loss of strength at slightly elevated temperatures (200 -- 300° F) and poor creep resistance. It is for such applications that Zn-graphite composites appear to be attractive. Kendall has reported the liquid metal infiltration technique coupled with hot-compacting for making the Zn-graphite composites [36]. He reported strengths of the composite as high as 88 percent of the rule-of-mixture prediction.

Fabrication of graphite-reinforced metal matrix composites can be accomplished without degradation of the fibers providing temperatures

are kept below 800° C. Thus, it is probable that reinforced Mg, Zn, Pb, and Al can be fabricated by molten-metal infiltration. However, higher melting point materials might be difficult due to reaction between wetting agent (Ni) and fibers. Thus, reinforced Cu, Fe, and Ni would be difficult to fabricate since temperatures must be held below 800° C or barrier coatings must be used.

CHAPTER III

EXPERIMENTAL TECHNIQUE

Experiments were conducted for the purpose of determining means of alleviating the incompatabilities in metal matrix--graphite fiber composites. Aluminum-graphite, zinc-graphite, and lead-graphite systems were chosen for the study, for the reasons explained in the previous chapter. Nickel, used as a wetting agent, and aluminum are representative of the two types of incompatabilities, i.e., graphite fiber recrystallization and carbide formation, respectively. Zinc and lead are representative of the third type of incompatability, lack of fiber wetting.

Two approaches were taken to reduce recrystallization in the nickel-graphite system: (a) coating the fibers with a more stable material, and (b) altering the fiber surface energy to make it more stable. The coatings employed were pyrolytic graphite, pyrolytic graphite with a high-temperature graphitizing heat treatment, and vitreous carbon. Various oxidizing treatments were given to fibers to improve the surface stability.

The liquid metal infiltration technique was used to fabricate the graphite-Al, graphite-Zn, and graphite-Pb composites. Since graphite fibers are not wet by liquid metals, the nickel coating was used as a coupling agent to improve the wetting of the fibers.

Nickel-Graphite

The graphite fibers used in the investigation were dog-bone shaped, PAN-based fibers produced by Great Lakes Carbon Corporation in 40,000 and 60,000 fiber tows. These fibers were Fortifil 3 (360 ksi tensile strength, 30 msi modulus) and Fortifil 5 (400 ksi tensile strength, 48 msi modulus). In addition, high-modulus, pitch-based fibers in the form of a 2,000 fiber-twisted tow and pyrolytic graphite-coated graphite mono-filament, supplied by Union Carbide and AVCO, respectively, were used.

Electrolytic nickel was deposited on individual bare or pyrolytic-coated fibers in a multifiber tow from a Watts bath. As seen in Figure 8, a uniform coating of approximately 2μm thick was achieved on each fiber.

Heating of nickel-coated fibers, both as received and surface treated, was performed in an alumina tube inserted through a cylindrical graphite resistance-heated furnace, shown in Figure 9. The heating was done in a vacuum of about 10^{-2} torr. The effects of elevated temperature exposures on the nickel-coated fibers were determined by measurement of pre- and post-exposure strength. The fracture strength (breaking load/original area) at room temperature of individual graphite fibers, as nickel-coated and after-heat treatment (at 600° to 1,100° C; time period: 1 to 24 hours) was determined. Each fiber was mounted with cyanoacrylate on a thin cardboard holder,

with, approximately, a one-inch guage length, and pulled to fracture at a cross-head speed of 0.02 inch/minute, using an Instron tensile testing machine. The effects of the isothermal exposures on the structure of the nickel-coated graphite fibers were assessed by mounting them in plastic, sectioning transversely, polishing and observing under an optical microscope.

The methods used to deposit carbon coatings on individual graphite fibers in tows were thermal decomposition of hydrocarbon gases, sputter coating, and pyrolysis of organic coatings. In order to obtain a low-surface energy coating, the pyrolytic carbon must be highly graphitic and highly oriented with the low-energy planes parallel to the surface [37]. The structure and properties of pyrolytic carbon obtained by chemical vapor deposition from hydrocarbon gases depend upon the geometry of the substrate, the deposition temperature, the type of gas used, the gas-flow rate, and the impurities in the gas stream [37]. Riley observed that using temperatures below 1,700° C results in deposits of fairly disordered carbon characterized by moderate orientation and small crystallite size while temperatures above 2,300° C result in highly graphitic structures with very high degrees of orientation. Heat treating of pyrolytic graphite at temperatures between 2,300° C and 2,800° C results in decreased c-spacing, growth in the a-b directions, and increased orientation [37].

A pyrolytic carbon-coating apparatus was designed, as shown in Figure 10, to coat resistively-heated graphite fibers. The apparatus consisted of a tubular glass chamber in which a bundle of graphite

fibers was resistively heated. Nitrogen was used as a carrier gas at a flow rate of 1.5 ft^3/hour (measured by a rotameter-type flow meter) and propane (.025 ft^3/hour) as the hydrocarbon gas source. Deposition time was about 30 seconds. The current was adjusted to raise the fiber temperature of 1,300° C. The pyrolytic carbon deposited on the fibers was approximately 1.2μm thick. There were some problems encountered using this method for coating. The graphite fibers were not uniformly coated because of nonuniform heating of fibers and nonuniform gas concentration through the bundle. Much of the coating was in the outer portion of the bundle with many fibers joined together by a solid deposit matrix. A flotation method employing a gas jet to create fiber movement during deposition was considered to improve these problems, but because of lack of facilities, no further work was done using this deposition technique.

Vitreous carbon coatings were obtained by carbonization of polymer resins. The graphite fiber tow was brushed with epoxy and allowed to cure in air. The epoxy-coated fiber tow was then carbonized at 1,200° C in an argon atmosphere, using a resistance-heated furnace.

Fortifil 5 fibers were sputter-coated with carbon, using the mini-coater made by Commonwealth Scientific. Individual fibers were taped to a steel frame and sputter-coated on each side, at 10 milliamp current in an argon atmosphere (35 micron pressure) for 2.5 minutes.

The graphite mono-filaments coated with pyrolytic graphite, obtained from AVCO, were sent to Great Lakes Carbon Corporation, where they were heated at 2,700° C for one hour in a nitrogen environment.

The purpose of this heat treatment was to further graphitize the pyrolytic coating.

The object of the various fiber-coating processes was to protect the fibers from recrystallization in contact with metals at high temperatures. Experimentation revealed that proper coating of individual fibers in fiber bundles could not be obtained because of the lack of necessary facilities. Therefore, subsequent fabrication studies were conducted without the use of carbon barrier coatings on graphite fibers.

Aluminum-Graphite, Zinc-Graphite, and Lead-Graphite

The liquid metal infiltration technique of fabricating composites has certain advantages over the hot-compaction technique. These are: (a) low cost, (b) ease of forming complex shapes, and (c) elimination of high lateral pressures, which can lead to fiber breakage. Since graphite fibers are not wet by molten metals, electroplated nickel was used in the present study as a coupling agent to promote wetting. Nickel-coated Fortifil 3 and 5 fiber tows obtained from the Great Lakes Carbon Corporation were used for the fabrication of the composites. The transverse micrograph of nickel-coated Fortifil 5 fibers is shown in Figure 11 (coating thickness, approximately 1μm). Two techniques, wire drawing and casting, were used to fabricate the composites.

The experimental equipment, which was developed to fabricate composites by a wire drawing technique using the apparatus shown schematically in Figure 12, was based on a semi-continuous fabrication principle: In an argon atmosphere, nickel-coated graphite fiber tows were drawn through a die at the bottom of a graphite crucible

containing the melt, at a speed of approximately 0.19 inch/minute. The composite wires so obtained were four inches long and 0.12 inch in diameter.

A casting technique was developed for fabricating graphite-7075Al alloy, graphite-Pb-2 percent Sn alloy, and graphite-Zn-2 percent Sn alloy composites. The Pb-2 percent Sn and Zn-2 percent Sn alloys were made using Pb (99.99 percent), Zn (99.97 percent), and Sn (99.99 percent). Tin was added to increase the fluidity of the melt. In each case, nickel-coated graphite fibers were cleaned in methyl ethyl ketone (MEK) to remove any contaminants. The fibers were then laid in a graphite mold, as shown in Figure 13. The alloy metal pieces were put in the hopper of the mold denoted "A" in the figure, and the mold was placed inside a two-inch internal diameter steel tube, which was placed in a resistance-heated tube furnace. A thermocouple touching the top surface of the mold was used to control the mold and casting temperature. Casting temperatures of 700° C, 330° C, and 420° C were used for C-Al, C-Pb, and C-Zn, respectively. For all three systems, the time of stay at casting temperature was five minutes. The chamber was purged with argon gas throughout the process. Commercially available fluxes were used to dissolve any metal oxides and to improve the wettability of the nickel coating by the melts. Various structural shapes, including I-sections, tubes, plates, and rods, were fabricated of graphite-7075Al, as shown in Figure 14. For the present study, the specimens fabricated were rectangular in shape with dimensions of four inches long, 0.4 inch wide, and 0.25 inch thick, and volume fractions of fibers varying between 0.13 and 0.33.

The graphite-7075Al specimens fabricated were directionally solidified in order to alter the morphology of the Al-Ni intermetallic. For the purpose of directional solidification, a zone-melting technique was used. The zone-melting unit used for the study is shown in Figure 15. This was a Westinghouse 10 kHz, 150 kw induction-heated zone refining unit. Figure 16 shows the specimen mount with the specimens used in the zone-melting unit. The unit consisted of a chamber in which the specimen was mounted vertically under a small tensile load. An inert helium atmosphere was maintained in the chamber. A stationary disc-shaped induction coil, two inches ID and 0.25 inch thick, produced a molten zone about 0.3 inch thick. The molten zone was passed by moving the specimen at various rates (2.5 inches to 27 inches/hour) through the length of the specimen in a direction parallel to the fibers. The test specimens were then prepared by machining away only that material necessary to provide parallel surfaces.

Mechnical Property Measurements

The tensile strength and elastic moduli of the composites were determined using an Instron Universal testing machine having a 10,000 pound load capacity. Glass fiber reinforced plastic grip tabs (0.375 x 1.5 inches) were glued to each end of the specimens with an epoxy adhesive to prevent crushing and premature failure of the test pieces in the jaws of the test machine.

Some of the test specimens were instrumented with strain gauges and the remainder with a strain gauge extensometer of 0.5 inch gauge length for the measurement of the composite strain used to calculate

elastic tensile modulus. The response of these gauges was monitored as a continuous trace on the strip chart of the test machine. Figure 17 shows a test specimen, with extensometer attached, mounted in the tensile machine. Measurements with the extensometer were within 10 percent of those obtained using strain gauges. This large discrepancy was due largely to great variability of properties among the specimens, and the fact that most measurements were made by extensometer and, relatively, very few with strain gauges.

Physical Property Determination

Prior to mechanical testing, the width and thickness dimensions of each specimen were measured with a micrometer. These dimensions, taken as the average of three readings along the specimen length, gave the cross-sectional area needed for the determination of stresses and moduli.

The volume fraction of fibers in each type of composite was determined by two methods:

1. The number of fibers was counted and averaged in micrographs at known magnification of different transverse cross-sections of the composite. Knowing the mean dimensions of the fibers, the total area of fibers in the section was calculated, which divided by the total area of the cross-section, gave the area fraction of fibers equal to the volume fraction.
2. A portion of composite specimen was weighed in air. The matrix was dissolved in concentrated nitric acid and the remaining residue was filtered. The fibers were dried in an

oven and weighed. The volume fraction of the fibers was determined by the equation:

$$\text{Volume fraction of fibers} = \frac{W_f/\rho_f}{W_f/\rho_f + W_a/\rho_a}$$

where

W_f = Weight of fibers

W_a = Weight of the matrix metal or alloy

ρ_f = Density of fiber

ρ_a = Density of matrix metal or alloy

The density of the composite was measured using the Archimedes method, which consists of weighing the sample first in air, and then submerging in a liquid of known specific gravity. The liquid used was methyl ethyl ketone, which thoroughly wet the material. The electronic balance used to make the measurements could be read to an accuracy of $\pm$ 0.00001 gram. The density was calculated using the formula:

$$\rho = \frac{W\rho_{MEK}}{W + H - S}$$

where

W = Weight of sample in air

H = Weight of sample holder in liquid

S = Weight of sample holder and sample in liquid

ρ_{MEK} = Density of MEK = 0.802 gm/cm^3.

The presence of voids may introduce considerable variability and uncertainty in density measurements. If all voids are sealed so that liquid penetration does not occur, the true bulk density is obtained.

If all voids are filled by the liquid, the true net density is measured. If an unknown fraction of the voids are penetrated by the liquid, the density measured lies somewhere between the two extremes. This situation existed in the present study.

Metallographic Observations

Both qualitative and quantitative studies were made of specimens using an optical microscope. Sections of specimens were mounted in plastic, ground and polished for observation of transverse and longitudinal microstructures. Photographs were taken of these microstructures. Also the scanning electron microscope was used to study the fracture morphology of the composite specimens. The purpose of metallographic observation is to correlate the metallographic observations to the measured properties.

CHAPTER IV

EXPERIMENTAL RESULTS

Nickel-Graphite Fiber System

As a base for experimental attempts to study the extent of grahpite fiber recrystallization, received fibers, plated with nickel, were given isothermal exposures at various temperatures for determination of the extent of degradation. The nickel-coated Fortifil 5 fibers were heated at 850° C in a vacuum of 10^{-2} torr for two hours. Microscopic examination, Figure 18, showed that nickel still surrounded each fiber and the geometry of the fibers was unaltered. Thus, it was concluded that recrystallization had not occurred. Conversely, heating at 1,000° C for one hour in a vacuum produced reaction zones as indicated by arrows in Figure 19. These consist of islands of nickel surrounded by areas of graphite that is considered to be recrystallized fiber. Heating the Fortifil 3 and 5 fibers for one hour at 1,100° C resulted in complete recrystallization. Evidence of this is shown in Figure 20, where the entire fiber is observed to be precipitated on the outside and the nickel having migrated into the center. The same phenomenon occurred when pitch precursor fibers were heated to the same temperature. In this case, the recrystallized appearance is as shown in Figure 21. The effect of the isothermal exposure on the strength of the nickel-coated Fortifil 5 fibers is shown in Figure 22, a decrease being indicated between ambient temperature and 1,100° C, at which the strength is nearly zero.

The first attempt to reduce the extent of graphite fiber recrystallization in the presence of nickel at elevated temperatures was by slight oxidation of the fibers to remove high-energy surface sites. The Fortifil 5 fibers were oxidized in partial vacuum (ranging from 10 to 40 mm Hg) and in air, at 1,100° C for one hour. After the oxidation treatment, graphite fibers were nickel-plated and heated at 1,100° C in a vacuum (10^{-2} torr) for one hour. The fibers oxidized in partial vacuum still recrystallized in the presence of nickel as shown in Figure 23a, b, c. The recrystallization zones are indicated by arrows in the figures. There was no apparent change in the extent of recrystallization over the range of partial vacuum used. However, there was no recrystallization of the fibers oxidized in air as evident from Figure 24. The oxidation treatment showed considerable strength degradation as evidenced by the ease with which the fibers broke on handling. For this reason, no further study was made of this effect.

The second modification to reduce recrystallization in the graphite-nickel system was by coating the graphite fibers with a layer of carbon. Fortifil 5 fibers sputter-coated with carbon a few Angstrom units thick, nickel-plated and heated at 1,100° C in a vacuum (10^{-2} torr) for one hour, showed no recrystallization as evident from Figure 25. The next experiment consisted of coating the Fortifil 5 fibers with pyrolytic graphite. Again, the nickel-plated fibers showed no recrystallization in the presence of nickel heated for one hour at 1,100° C in a vacuum (Figure 26). Furthermore, Fortifil 5 fibers, carbon-coated by carbonizing an epoxy resin applied to the surface,

showed no recrystallization by nickel at 1,100° C (Figure 27). Possible mechanisms for the effectiveness of these carbon barrier coatings are discussed in the next chapter.

The transverse microstructure of graphite mono-filaments, coated with graphitized pyrolytic carbon, showed no recrystallization of the graphite filaments in the presence of nickel, heated at 1,100° C in a vacuum for 24 hours (Figure 28). The strength test results for the mono-filaments after annealing at various temperatures (800° C to 1,200° C) for two hours in a vacuum (10^{-2} torr) are shown in Figure 29, with little or no strength degradation having occurred at any temperature.

Composite Mechanical Properties

The measured longitudinal ultimate tensile strengths and elastic moduli of as-cast Fortifil 3 and 5 graphite fibers-7075Al, Pb-2 percent Sn alloy, and Zn-2 percent Sn alloy, are given in Table IV as functions of fiber volume fraction.

It may be seen from the Tables and Figures 30 and 31 that strength and modulus values of the composites increase with increasing volume fraction of fibers. For example, in the case of Fortifil 3 graphite-aluminum, the ultimate tensile strength increased from 17.1 to 20.1 ksi as the volume fraction of fibers increased from 0.12 to 0.22. The tensile modulus increased from 12.6 to 18.1 msi over the same range of volume fraction. In the case of Fortifil 5 graphite-7075Al, although based on only two data points, it appears that composite strength value increases to a certain volume fraction; beyond which, it decreases.

According to the results obtained, this transition must lie somewhere between 22 and 33 volume percent.

The factors controlling the growth morphology of Al_3Ni into fibrous or planar form are (a) the thermal gradient at the solid-liquid interface, and (b) growth rate [32]. In the present study, it was not possible to vary the thermal gradient during directional solidification because of the equipment limitations. The equipment used had no means of cooling the composite specimen from one end to increase the thermal gradient. Hence, only the growth rate effect on the strength of the Fortifil 5-7075Al composite was studied. The composite contained 13 volume percent fibers. Atomic absorption chemical analysis of the matrix showed that it contained about 13.2 weight percent nickel. The measured variation of the tensile strengths and the moduli with growth rate of Fortifil 5-7075Al composite are given in Table VI and Figures 30 and 31, with little strength variation being indicated.

Composite Densities

The experimental and theoretical density values are presented in Table V for graphite-7075Al, Pb and Zn composites. The experimentally measured density values are less than the theoretical, for reasons discussed in the next chapter. The theoretical values of 100 percent dense material were calculated from the rule of mixtures equation:

$$\rho_c = v_f\rho_f + v_i\rho_i + v_m\rho_m$$

where v is volume fraction and the subscripts f, i and m denote fiber, secondary phase, and matrix, respectively. For example, in the case of

lead-Fortifil 5 composite containing 10.96 volume percent fibers,

$$\rho_c = (0.1096)\ (1.8) + (0.048)\ (8.9) + (0.8904)\ (11.34) = 10.17_g/cm^3.$$

The fiber density was obtained from manufacturer's data, the density of nickel and lead from handbook values for the pure metals and the nickel volume fraction from optical measurements.

Metallographic Observations

Micrographs of transverse sections of graphite-7075Al, Pb, and Zn composites are given in Figure 32a, b, c. These micrographs illustrate that good infiltration of the fiber bundle had occurred. Thus, it was concluded that the graphite fibers were wet by the matrix.

The flatness of the fracture surface in the case of as-cast Fortifil 5-7075Al, Figure 33, shows the brittle nature of the fracture. As shown by the Orowan or modified Griffith equation for fracture [47]

$$\sigma_f = \left[\frac{2E(\gamma_s + \gamma_p)}{\pi c}\right]^{1/2}$$

where

σ_f = fracture stress

γ_s = elastic work of fracture

γ_p = plastic work of fracture, and

c = half crack length.

Brittle materials have much lower fracture strength than ductile ones because the plastic work of fracture may be very small, while for ductile metals, it is 10^5 - $10^6 erg/cm^2$, as compared to values of elastic work of fracture, γ_s, of about 1,000 - 2,000erg/cm^2. As

predicted by the above equation, low experimental strength values (13.2 ksi for 13 volume percent Fortifil 5-7075Al) were, in fact, obtained. Figure 34 shows the crack propagation through the brittle Al_3Ni. Metallographic observation of the directionally solidified Fortifil 5-7075Al composite shows the change in the microstructure of the composite along the length of the specimen. Figure 35a is the longitudinal micrograph of the as-cast specimen at the bottom where no zone was passed (brittle phase randomly oriented); Figure 35b is the micrograph of the middle of the specimen (brittle phase alligned); and Figure 35c represents the micrograph of the end of the specimen where the molten zone exited (brittle phase broken into smaller size and aligned). SEM observation of the fracture surface, Figure 36, of directionally solidified graphite-Al composite showed the ductile nature of failure of the matrix, resulting from increased spacing between the Al_3Ni rods in the ductile aluminum matrix as compared to the almost continuous network of Al_3Ni in as-cast. For 13 volume percent fibers, the average composite strength was 32 ksi. The longitudinal micrograph, Figure 37, of directionally solidified graphite-Al composite, at slower rates (2.5 inches/hour), showed the aluminum carbide formation, indicated by the arrows, resulting in lower strength (20 ksi) probably due to reduced fiber strength caused by surface carbide formation.

CHAPTER V

DISCUSSION

Nickel-Graphite System

The approaches taken in this investigation to decrease the extent of fiber recrystallization were based on the mechanisms for the process as set forth by other investigators. Brophy, et al., [38] have proposed a mechanism for the recrystallization of individual nickel-coated graphite fibers. Thin nickel coatings have been observed to spherodize during heat-treatment at high temperatures. The driving force for this process is the reduction in nickel-surface energy, and it would tend to take place at temperatures where nickel self-diffusion is significant (> 1/2 melting temperature). Once the nickel coating has been converted to small spheres, a further reduction in the nickel surface energy can only be achieved by the coalescence of small spheres to form larger spheres. This can occur by the movement of carbon atmos through the nickel during fiber recrystallization, causing a net movement of the nickel towards the recrystallized fiber center. They observed that the more graphitized fibers resist recrystallization better than carbonized fibers, because their more orderly, more stable, structure is more resistant to dissolution in the nickel.

According to Shiota and Watanabe [14], there are many crystallites having various lattice spacings in the graphite fiber. Crystallites, having more narrow spacing, would have lower free energy than wide ones. According to this model, the diffusion of carbon atoms through nickel is

caused, not simply by a gradient of concentration of carbon atoms in the nickel, but by this difference of free energy on the fiber surface. Instrusion of nickel into the fiber takes place initially by diffusion of carbon atoms from less graphitized crystallites in the graphite fiber to more graphitized crystallites and growth of graphite at those crystallites should cut off a part of nickel from the coated nickel layer. The process goes on until the entire fiber is consumed.

Thus, according to this mechanism, if the surface free energy of the graphite fiber is made homogeneous by some treatment, the reaction between carbon and nickel will be prevented. The fiber oxidation experiments in this investigation showed considerably improved fiber stability, thereby tending to support the validity of the Watanabe mechanism. On the same basis, it was thought that if the graphite fibers were coated with a carbon having a more chemically homogeneous surface (little variation of surface free energy), the fiber stability may be increased. In order to investigate this, the recrystallized Fortifil 5 fibers were recoated with nickel, using a Watts bath, and heated at 1,100° C for 10 hours in vacuum (10^{-2} torr). There was no further recrystallization of the outer graphite layer, Figure 38, which is thought to be chemically homogeneous [4]. Hence, the various carbon barrier coatings showed promising results.

The effectiveness of barrier coatings in preventing fiber damage by limiting carbon diffusion into the matrix increases with the coating thickness, according to Fick's law. However, as described in Chapter II, a critical thickness, t_{ℓ}^{*}, of brittle coatings exists beyond which the

fiber strength is degraded by the introduction of large numbers of flaws, according to the equation

$$t_\ell^* = \left[(d/2)^2 + t_\ell(d + t_\ell)(E_f\sigma_{u\ell l}/E_\ell\sigma_{uf})^\beta\right]^{1/2} - d/2$$

For the case of a pyrolytic graphite coating, values of $\sigma_{u\ell l}$ = 45 ksi and E_ℓ = 4.6 msi are taken from reference [40]. Values of β for brittle materials typically range from two to five [21]. Using a midrange value of 3.5 for β, and taking σ_{uf} = 400 ksi, E_f = 48 msi and d = 8μm for Fortifil 5 fibers (manufacturer's data), t_ℓ^* is calculated to be 11.4μm. As seen from Figure 26, the pyrolytic graphite coating that was applied was approximately 1.5μm thick, far below the calculated critical value.

Composite Fabrication

Uncoated graphite fibers are not wet by liquid melts. Wetting occurs when the respective surface free energies noted in the energy balance equation (page 16) combine to produce a contact angle between melt and the graphite fiber of less than 90 degrees. Naidich has reported contact angles of 156° and 138° for molten aluminum (800° C) and lead (800° C), respectively [24], on graphite surface. Thus, it would not appear possible to produce graphite reinforced Al or lead by molten metal infiltration. In the present study, electroplated nickel, as previously used by Sara [23], was used as a coupling agent to improve the wetting of graphite fibers by the melt. The process governing the wetting is the relative surface energy or surface tension. From the observation that wetting occurred, introduction of the nickel coating obviously increases γ_{sv} such that $\gamma_{sv} > \gamma_{s\ell}$ in Figure 7, the necessary

condition for wetting to occur. Thus, the nickel coating serves the critical function enabling the liquid metal to infiltrate into the fibers.

Aluminum-Graphite

From the observation that wetting does occur, the surface energy of the nickel coating is evidently greater than that of the alloy melt in contact with nickel ($\gamma_{s\ell}$). Infiltration of the fibers by the aluminum matrix occurs due to the combined effects of capillary action and gravity. For the 7075 Al alloy, a melt temperature of 700° C was used, 62° C above the 638° C liquidus temperature to increase fluidity. Diffusion of nickel into the 700° C melt begins immediately upon contact. According to Eremenko, et al., [41], the dissolution rate of nickel in molten aluminum is 6.9×10^{-5} m/second at 700° C. Data reported by Reick, et al., [42] indicate that a 1μm thick nickel layer such as that present on the fibers used in this investigation would be dissolved in about one second. Thus, within one second of contact, the weight percent nickel in the matrix of a composite containing 13 volume percent fibers is 13 weight percent. From the phase diagram [41], Figure 39, at 700° C, the system would consist of liquid aluminum saturated with about 5 weight percent nickel and precipitated Al_3Ni intermetallic. Bare graphite fibers are not wet by molten aluminum. However, since wetting was evidently maintained long enough for infiltration and complete solidification to occur, the equilibrium 13 weight percent nickel solution was apparently not present. Either infiltartion occurred in less than the one second required to dissolve the nickel coating or a thin film of Al_3Ni was maintained on the fiber.

Zinc-Graphite and Lead-Graphite Composite

The process governing the solidification of the graphite-Zn composite is probably similar to that of the graphite-Al, since, at casting temperature, both systems consist of nickel saturated metal plus an intermetallic (see Figure 40). For the zinc system, this would be $NiZn_8$ up to about 13 weight percent Ni. The intermetallic is indicated by arrows in Figure 32c. However, the micrograph of the graphite-Pb composite, Figure 32b, shows the nickel coating around the fibers and not dissolved into the lead matrix. The lead-nickel equilibrium diagram [41], Figure 41, shows a very low solubility of nickel in lead. So in this case, the nickel coating acts only as a coupling agent to improve the wetting of graphite fibers by molten lead, and the solidification of the lead matrix takes place when the composite is cooled in the die.

Calculation of Nickel and Fiber Content

Nickel content of the composite was calculated by the procedure given below, using the graphite-Al system as an example. A tow of Fortifil 5 contains nominally 40,000 fibers, each of approximately 65 x $10^{-8}cm^2$ area (manufacturer's data). Each fiber has an approximate 1μm thick nickel coating on it. The area of the composite made is 0.1 $inch^2$ (0.4 x 0.25 inch) or 0.64cm^2.

The volume of the specimen per unit length is, therefore, 0.64cm^3.

Average Area of one Fortifil 5 fiber = 65 x $10^{-8}cm^2$.

Average Area of the fiber + 1μm thick nickel coating = 9.13 x $10^{-7}cm^2$.

Three tows of Fortifil 5 fibers were used to make the composite.

Average Area of 3 fiber tow (each of 40,000 fibers) = $0.078cm^2$.

Therefore, Average Volume occupied by these fibers (1cm long) = $0.078cm^3$.

Average Area of nickel coating = $9.13 \times 10^{-7} - 65 \times 10^{-8}$

$= 2.63 \times 10^{-7} cm^2$.

Average Area of nickel coating on 3 fiber tows = $0.031.cm^2$.

Average Volume occupied by nickel = $0.031cm^3$.

Total Volume occupied by fibers and nickel = $0.109cm^3$.

Volume of the mold or composite = $0.64cm^3$.

Therefore, Volume occupied by 7075Al alloy = $0.531cm^3$.

Weight of 7075Al alloy = 0.531 x 2.8 (density of 7075 Al alloy)

= 1.486 gms.

Weight of nickel = 0.031 x 8.9 (density of nickel)

= 0.275 gms.

Therefore, total weight of Ni + 7075Al = 1.761 gms.

Weight percent Ni in alloy = $\frac{0.275}{1.761} \times 100$ = 15.61 percent.

The weight percent Ni in the alloy determined experimentally was 13 percent. The difference in the results may be due to the uncertainty in the fiber coating areas caused by the variability of the fiber shape,

as evidenced by Figure 11 and the voids in the matrix. Similarly, the volume fraction of fibers in the composite can be calculated theoretically. In the above case

Average Volume of 3 tows of Fortifil 5 fibers = $0.078cm^3$.

Volume of the mold composite = $0.64cm^3$.

Therefore, Volume fraction fibers in composite = $\frac{0.078}{0.64}$ = 12.18 percent.

Experimentally, the value was found to be 13 percent. Again, the difference in two values may be due to variation in the fiber area.

The density of a composite that contains no voids is computed using the rule of mixtures method, which is

$$\rho_c = v_f\rho_f + v_i\rho_i + v_m\rho_m$$

where

ρ_c = Density of the composite, gm/cm^3

v_f = Volume fraction of fiber in the composite

v_i = Volume fraction of Ni or intermetallic in the composite

v_m = Volume fraction of matrix

ρ_f = Density of fiber, gm/cm^3

ρ_i = Density of Ni or intermetallic, gm/cm^3, and

ρ_m = Density of the alloy.

The difference between calculated and measured composite densities is due to porosity, which is obvious from the transverse micrographs of the composites.

Void Fraction

The volume fraction of voids in the composite is calculated as follows: Since the composite is made of fibers and matrix, the mass M_c is the sum of the total mass M_f of fibers and the mass M_m of matrix.

$$M_c = M_f + M_m$$

The above equation is valid regardless of voids. However, the composite volume V includes the volume V_v of voids so that

$$V_c = V_f + V_m + V_v$$

Now density of the composite is

$$\rho_c = \frac{M_c}{V_c} = \frac{M_c}{V_f + V_m + V_v}$$

Dividing the RHS by M_c, and since density = Mass/volume $V_f = M_f/\rho_f$ and $V_m = M_m/\rho_m$.

$$\rho_c = \frac{1}{\frac{M_f}{M_c}\frac{1}{\rho_f} + \frac{M_m}{M_c}\frac{1}{\rho_m} + \frac{V_v}{M_c}}$$

where

$\frac{M_f}{M_c} = m_f$ (mass fraction of fiber in the composite)

$\frac{M_m}{M_c} = m_m$ (mass fraction of matrix in composite)

$$\rho_c = \frac{1}{\frac{m_f}{\rho_f} + \frac{m_m}{\rho_m} + \frac{V_v}{V_c}\frac{1}{\rho_c}}; \quad M_c = \rho_c V_c$$

where $\frac{V_e}{V_c} = v_v$ (volume fraction of voids)

$$\rho_c = \frac{1}{\frac{m_f}{\rho_f} + \frac{m_m}{\rho_m} + \frac{v_v}{\rho_c}}$$

Rearranging the above equation gives

$$v_v = 1 - \rho_c \left(\frac{m_f}{\rho_f} + \frac{m_m}{\rho_m}\right)$$

This equation was used to calculate the void fraction of the composite as given in the last column of Table V, varying between 1 and 13 volume percent. These voids were introduced by trapping of gas in the melt as it flows into the fibers. Nickel coating around clusters of fibers with enclosed gas pockets may also be a source of voids.

Mechanical Properties

The major load bearing phase in fiber reinforced composites is the fibers. A principal function of the matrix is to transfer load to the fibers by a shear mechanism. For effective transfer of stress the modulus of the matrix must be lower than that of fibers. It is also desirable that the matrix be as tough as possible so as to impede crack propagation.

The ultimate tensile strength and the modulus of elasticity of composites is represented by the following equations which define the rule of mixtures (ROM) relationships:

$$\sigma_c = \sigma_f v_f + \sigma_m v_m$$

where

σ_c, σ_f = Ultimate tensile strength of the composite and fibers, respectively;

σ_m = Stress on the matrix at the equivalent strain at which the ultimate tensile strength of the fibers is achieved; and

v_f, v_m = Volume fraction of the fibers and matrix, respectively, and

$$v_m = 1 - v_f$$

The ROM relation was shown to be valid for the ultimate tensile strength of continuous-metal fiber, metal-matrix composites by Jech, et al., [42]. Subsequently, they demonstrated that the ROM relationship was also valid for the elastic modulus (E) of these composites. The ROM relationship for elastic modulus is represented as follows:

$$E_c = E_f v_f + E_m(1 - v_f)$$

where

E_c = Elastic modulus of the composite

E_f, E_m = Elastic moduli of the fiber and matrix, respectively.

Certain assumptions are inherent in these relationships and are summarized as follows:

1. The composite, the matrix, and the fibers undergo equal strain for a given load on the composite;
2. The bonding between the matrix and the fibers is perfect;
3. The fibers are aligned parallel to the tensile axis;
4. The strength of the fibers does not vary, i.e., no scatter;
5. The properties of the matrix and the fibers are identical in-situ (as they exist within the composite), as they are when the matrix and the fibers are tested in their uncombined forms;
6. No residual stresses exist in the matrix or the fibers, prior to loading the composite;
7. The Poisson ratio of both fiber and matrix are equal.

The above treatment neglects some significant features of the strength of fibers, such as the variation of strength from fiber to fiber. Thus the choice of σ_f in the last equation is far from obvious, and it is necessary to use a statistical approach to determine the bundle strength. It is well known that the experimentally measured strengths of brittle solids are subject to large amounts of scatter which can be described by the Weibull distribution function [21]. This approach can also be used for brittle graphite fibers. When the strength of a large number of brittle fibers, diameter d, is measured over a test gauge length l, the distribution of strengths can be represented by the Weibull distribution function. The Weibull distribution curve has two

cut-off points corresponding to a lower-strength limit σ_l, and an upper-strength limit σ_u. The latter is equivalent to the theoretical strength of the fiber in the absence of any internal defects or surface flaws which are responsible for the reduced strengths. The Weibull cumulative probability distribution function $G(\sigma)$ is given by

$$G(\sigma) = 1 - \left[1 - \left(\frac{\sigma - \sigma_l}{\sigma_0}\right)^m\right]^\omega \qquad (5\text{-}1)$$

and is the probability of fracture of a fiber at a stress level equal to or less than σ. In this equation $\sigma_0 = \sigma_u - \sigma_l$, ω is $1/d$ and m depends on the amount of scatter. The mean strength of fibers is given by

$$\bar{\sigma} = \sum_{i=1}^{N} \sigma_i / N \qquad (5\text{-}2)$$

where σ_i is the strength of individual fibers. The fracture strength of a bundle of fibers σ_b which, as individual fibers exhibit the distribution described by Equation (5-1), and have a mean strength $\bar{\sigma}$, was derived by Coleman [43]. For this derivation, it is assumed that the fibers in the bundle are separated from each other and have the same cross-sectional area. At all stresses below σ_l, the fibers have the same elongation and are unbroken. As the load is increased, the weakest fibers break in succession and the load is taken up by the unbroken fibers. The maximum or breaking load of the bundle occurs when the stress on the remaining fibers reaches σ_u and complete fracture occurs. Coleman found that σ_b is less than $\bar{\sigma}$ and that the ratio $\sigma_b/\bar{\sigma}$ depends on the amount of scatter in the strength of the individual fibers according to

$$\frac{\sigma_b}{\bar{\sigma}} = \left(\frac{1}{me}\right)^{1/m} \frac{1}{\Gamma(1 + 1/m)}$$

where Γ is a tabulated gamma function. He observed that for brittle fibers, which usually show a large amount of scatter and have values of m between 2 and 5, the bundle strength is 50 - 65 percent of the mean strength. Assuming this applies for graphite fibers, the bundle strength would be 200 - 260 ksi for one inch long Fortifil 5 fibers ($\bar{\sigma}$ = 400 ksi, manufacturer's data). The value used for bundle strength in all calculations in this work is 260 ksi.

As seen from Table IV, the ROM strengths are generally well above the experimental values. The most likely causes for the lower strength are the existance of voids in the matrix and of fiber misorientation to the load axis. These effects are discussed below. It may be noted that Fortifil 5-Zn composite strengths are quite near the ROM values as expected from the low void fractions of one to two percent. In contrast, the lead matrix composites with more than 10 percent voids (Table V) show strengths much below the ROM.

Effect of Voids on Strength

The effect of porosity or voids on the strength of the composite will depend on the fiber fracture or the matrix cracking (if the matrix is brittle). The presence of voids represent a degree of unreproducibility in the strength numbers, perhaps because of variation of void shape and distribution. For simplicity, two extreme conditions (upper and lower strength limits) can be specified; these are discussed below.

The actual composite tensile strengths are expected to lie between the two extremes.

For the determination of the upper bound, consider that the composite member is divided into small approximately cylindrical volumes as shown in Figure 42 so that the fibers in these cylinders may be considered as individual bundles. The opportunity for the fibers in a small volume of the composite to behave like a bundle of unconnected fibers is introduced by the presence of voids in the composite. The voids displace the matrix only. Furthermore, the void distribution is non-uniform. A local region with a high void density may correspond to one of the small cylindrical void volumes introduced above. In these small volumes with high void density, the shear transfer through the matrix is effectively eliminated. The bundle fracture is anticipated in the weakest of these small volumes with high void density. Fracture of a fiber bundle occurs at a composite stress

$$\sigma_c = \sigma_b v_f$$

where σ_b = strength of the fiber bundle in the region of high void density. At some upper value of bundle strength, all bundles created by voids will have failed, as depicted in Figure 42. Then the upper limit of composite strength will be determined by the criterion of net section failure. The net section stress is given by

$$\sigma_{net} = \frac{\sigma_c}{1 - v_v}$$

where v_v is void fraction, assuming the voids to be uniformly distributed so that the fraction of voids is equal at all cross sections. For the case of the 21 volume percent Fortifil 5-7075Pb composite, σ_{net} is 62.4 ksi. As seen in Table IV, this stress is above the ROM composite strength, so that failure occurs when the void bundles fail. For many of the fabricated composites, calculation of σ_{net} yields below the ROM strength, probably because the void fraction was not actually uniform, so that failure occurred at areas of higher void fraction than the average value measured.

The actual strength of composite containing voids will be less than this upper bound due to the stress concentrating effect of the voids and of the cracks generated in the fibers and/or the matrix. The lowest composite strength will be for the case of a composite having a brittle matrix, as in the case of the as-cast aluminum-nickel. For the determination of the lower bound of the composite strength, voids of approximately spherical shape present in the matrix are assumed. In a member subjected to axial tension, the theoretical stress at the edge of an internal cavity, having the shape of a sphere, is raised from σ to 2.05σ [44]. It is assumed that the bond between the fiber and the matrix is perfect and that the matrix is brittle. If the bond is not strong, the fiber-matrix interface will break and the crack will stop propagating. The ultimate tensile strength of the as-cast Al-Ni eutectic alloy is around 13 ksi [32]. For an external stress of 13/2.05 = 6.3 ksi, the stress at the edge of the spherical void in the matrix will reach the ultimate and the crack will propagate in the composite leading to

failure. The measured composite strength for the Fortifil 5-7075Al was 8.9 ksi from Table IV, in fair agreement with the lower strength bound.

Effect of Fiber Orientation on Strength

In the present fabrication technique, although care was taken to maintain good fiber alignment with the tensile axis, some amount of misalignment is unavoidable. Some percentage of fibers is misaligned as shown in Figure 43 by arrows.

Consider the case when the fibers are at angle ϕ to the tensile axis as shown in Figure 44. According to Kelly and Davies, if the fibers are oriented at an angle ϕ to the applied stress σ, three possible modes of failure exist [45].

(1) For small values of ϕ, the matrix can flow in a direction parallel to the tensile stress axis until the fibers fail. The stress to produce this failure is

$$\sigma = \frac{\sigma_c}{\cos^2\phi} \tag{5-4}$$

where σ_c = ultimate tensile strength of the composite when $\phi = 0$;

(2) For intermediate values of ϕ, the matrix can fail in shear on a plane parallel to the fibers. The stress necessary to cause this type of failure is given by the equation

$$\sigma = \frac{\tau_u}{\sin\phi \cos\phi} \tag{5-5}$$

where τ_u = ultimate shear stress of the matrix with fibers;

(3) When ϕ is large, the matrix can fail by flowing in a direction transverse to the fibers. The stress that will cause this failure is given by

$$\sigma = \frac{\sigma_u}{\sin^2\phi} \tag{5-6}$$

where σ_u = ultimate strength of matrix in plain strain.

For very small angles of orientation, the first failure mode is critical. At a certain value, called the critical angle, the second mode becomes critical. This critical angle is given by

$$\phi = \tan^{-1}\left(\frac{\tau_u}{\sigma_c}\right)$$

If fiber misorientation in the produced composites is not spatially randomly distributed, but rather consists of clusters or entire tows of fibers misaligned at approximately the same angle, the effect will not be the same as for a random distribution. Nor would the failure stress of such a cluster probably be the same as that of a composite with fibers of equal orientation, because of restraint by the surrounding composite. However, if this restraining effect is assumed small, the failure stress of the clusters may be obtained from Equation (5-4) or (5-5), depending upon the angle. For example, for the 13 volume percent Fortifil 5-7075Al composite which failed at 13.2 ksi, the misorientation angle for a single cluster failure to have caused failure of the composite would be, 38 degrees from Equation (5-5), where τ_u is 6 ksi for graphite-Al composite [46], assuming the value is the same in the present case. Since microstructural observation did not indicate the

existence of fiber clusters with this high degree of misalignment, it is likely that failure occurred from the cumulative failure of numerous such misoriented fiber clusters, from the stress concentrating effect of voids (see previous section), or a combination of the two.

Graphite-Aluminum Composite

The volume fraction of Al_3Ni in the composite containing 13 weight percent Ni can be calculated using Lever arm principle. The equilibrium diagram indicates the composition of the phases that will be in equilibrium at any particular temperature. The diagram also makes it possible to determine the proportion of co-existing phases at any given temperature. Consider an alloy containing 13 weight percent Ni and 87 weight percent Al. At room temperature, as indicated in Figure 39, an equilibrium alloy is composed of Al and Al_3Ni (compound). Using the Lever rule, the amounts of Al and Al_3Ni are inversely proportional to the distances from the point representing the composition of the alloy (13 weight percent Ni-Al) to the points representing the composition of the phase in question (42.03 weight percent Ni in Al_3Ni). The weight fraction of Al_3Ni phase in the matrix is 13/42.03 = 0.30. The volume fraction of the components is calculated from their mass fraction and densities. With an Al_3Ni density of 3.98 gm/cm^3, the volume percent of Al_3Ni in the matrix is 22.69. Since the matrix occupies 87 volume percent of the composite, 19.74 volume percent of the composite is Al_3Ni.

The longitudinal tensile strength of the graphite-aluminum composites apparently increases to some volume fraction of fiber, Table IV,

but beyond that volume fraction, it decreases. The likely reason for this behavior is that as the fraction of fibers increases in the composite, the amount of nickel, and hence the proportion of the intermetallic phase, increases resulting in increased brittleness. The extent of embrittlement is dependent upon the shape and size of the brittle phase in addition to quantity, as will be discussed in the next section. For the 33.33 volume percent Fortifil 5 graphite-7075Al composite, the volume percent of Al_3Ni in the matrix and composite is calculated to be 72.07 and 48.04, respectively. The volume percent aluminum is only 18.6 as opposed to 81.37 volume percent brittle phase (fiber and Al_3Ni) under these conditions; a crack initiated by voids, fiber breakage or Al_3Ni breakage may readily propagate to catastrophic failure. The high volume percent and continuity of the Al_3Ni is apparent in Figures 34 and 35a. The flatness of the matrix fracture surface in Figure 33 reveals the occurrence of brittle fracture.

Effect of Directional Solidification

The improvement in strength of the composite after directional solidification is attributed to alteration of the intermetallic phase morphology. The directional solidification aligns the intermetallic parallel to the specimen axis, instead of being randomly distributed as in the as-cast composite, Figure 35a. The fractograph of the directionally solidified composite reveals ductile fracture of the matrix, Figure 36.

The influence of directional solidification on the ultimate tensile strength of graphite - Al-Ni composite is discussed below. In the

as-cast graphite-Al-Ni composite, Figure 35a, the intermetallic Al_3Ni (brittle) is in the form of large, irregularly shaped crystals in the matrix Al; but after directional solidification, Figure 35b, it is aligned approximately parallel to the tensile axis in rod form. Increase in the axial dimension, decrease in lateral dimension, and alignment of Al_3Ni intermetallic in the axial direction is contributing to the strength increase of the composite after directional solidification.

As stated before, the strength of brittle materials is affected by their volume according to the equation

$$\frac{\sigma_1}{\sigma_2} = \left(\frac{V_2}{V_1}\right)^{1/\beta}$$

According to Hertzberg, et al., [32], the average strength of 0.51μm diameter, 0.54 mm gage length, Al_3Ni whisker is about 292 ksi. In the case of graphite-Al-Ni composite after directional solidification, the area of Al_3Ni was found to vary between 200 to 800μm^2 and length between 300 to 600μm. According to the above equation, $\beta = 3$ [21], the strength of 200 x 300μm^3 Al_3Ni whisker is 36.53 ksi. The rule of mixture strength of the composite is given by

$$\sigma_c = \sigma_b V_f + \sigma_{Al_3Ni} V_{Al_3Ni} + \sigma_{Al} V_{Al}$$

For the case of graphite-Al_3Ni-Al composite containing 13 volume percent graphite fibers and 19.74 volume percent Al_3Ni directional intermetallic, taking $\sigma_{Al} = \sigma_{YAl} = 2.5$ ksi, the value of composite strength is 42.69 ksi. For graphite-Al_3Ni-Al composite containing 26 volume

percent Fortifil 5 graphite fibers and 38.76 volume percent Al_3Ni, the composite strength is 71.37 ksi, while average strength value experimentally obtained is 84.2 ksi.

The average value of the ultimate tensile strength experimentally obtained was 32 ksi. The reason for the lower value of the experimental ultimate tensile strength compared to ROM value is the voids present in the composite and misalignment of the fibers. The variation in growth rate or zone-passing velocity does not seem to affect the strength of the composite appreciably as seen in Table VI. The reason for this may be that the shape and size of Al_3Ni is nearly the same in all cases as apparent from Figures 35b and 43.

Statistical Comparison of As-Cast and Directionally Solidified Composite

In the present study, a statistical approach has been taken to assess the effectiveness of the directional solidification treatment to the as-cast graphite-7075Al composite in improving the tensile strength. The method used is called the Rank test. The procedure for the Rank test is as follows:

(1) Let n_i be the number of values in Group i;

(2) Let $N = \sum_{i}^{k} n_i$ be the total number of values;

(3) Rank each value from 1 to N beginning with the smallest. (If there are ties among t values, divide the successive ranks equally among them.);

(4) Compute r_i, the sum of the ranks for the ith group;

(5) Compute

$$T = \left[12/N(N + 1)\right]\left[\sum(r_i^2/N)\right] - 3(N + 1)$$

where the terms N and r_i are defined above.

(6) Go to Table VIII (Chi-square distribution); find the entry under k-1, where k is the number of methods being compared. If T exceeds the entry, then the data supports the conclusion that the groups are different. Otherwise, they are not different.

The data used for strength values is shown in Table VI for 13 volume percent graphite-Al composite, as-cast and directionally solidified (zone travel rate = 10 inches/hour). In Table VII, the numerical values representing ultimate tensile strength have been ranked from smallest to largest. The ranks are in parentheses in Table VII. The number of values in each group is 3; hence, $n_i = 3$. The total number of values N = 6. The sum of the ranks r_i for each group is shown in Table VII.

$$T = \left[12/6(6 + 1)\right]\left[\frac{261}{3}\right] - 3(6 + 1)$$

$$T = 3.8571$$

Here, tensile strength values are obtained using two methods; hence, k is 2. For k-1 = 2-1 = 1, the entry in the Chi-square distribution table is 3.841, which is less than T. Hence, the data supports the conclusion that directional solidification made a measurable difference on the tensile strength of the composite.

CHAPTER VI

CONCLUSIONS

(1) It may be concluded from these experimental studies that simple modifications to the nickel-graphite systems, such as carbon coatings and oxidative treatments to the fibers, are effective in improving the high-temperature structural stability of the system. The carbon-coating treatment appears especially promising. Applying the carbon coating would be expected to have other benefits, such as (a) improvement of the bond between matrix and fibers, and therefore, the composite strength, especially the interlaminar shear strength, (b) improvement of handleability, and (c) no increase in density of the fiber.

(2) The fabrication technique involving liquid metal infiltration of nickel-plated graphite fibers can be used to manufacture many kinds of structural shapes on a continuous basis with maximum strengthening efficiency. The process of fabrication will avoid fiber damage and produce a well-bonded matrix/fiber composite.

(3) The strength of nickel-aluminum-graphite fiber system composites can be improved by directional solidification of the composite.

CHAPTER VII

RECOMMENDATIONS

(1) Experiments are needed to find the best method of coating the grahpite fibers with pyrolytic carbon. The other coatings, such as alloys of pyrolytic graphite with boron and tungsten, in concentrations less than a few percent, should be tried to study the compatibility of nickel with them.

(2) A study should be made on the effect of the thermal gradient at the solid/liquid interface, during directional solidification, on the mechanical properties of graphite-aluminum composites. Also other coupling agents, such as copper, should be investigated. Other types of graphite fibers should be tried for fabricating the composite.

LIST OF REFERENCES

LIST OF REFERENCES

1. Berghezan, A.: Nucleus, 8, 5, 1966.

2. Javitz, A. E.: Design, January 18, 64, 1965.

3. LeMaistre, C. W., and R. J. Diefendorf: "The Origin of Structure in Carbon Fibers", Advanced Materials: Composites and Carbon, Amer. Ceramic Soc. Symposium, Chicago, 1971.

4. Riley, W. C.: "Graphite", Ceramics for Advanced Technologies, Ed. by Hove, J. E., and W. C. Riley, John Wiley & Sons, Inc., 1965.

5. Butler, B. L., and R. J. Diefendorf: "Graphite Filament Structure", Carbon Composite Technology Symposium, 10th Annual, Jan. 1970.

6. Wicks, B. J., and R. A. Coyle: "Microstructural Inhomogeneity in Carbon Fibers", J. Mat. Sci., 11, 376, 1976.

7. Butler, B. L.: "The Effects of Carbon Fiber Microstructure on the Shear Strength of Carbon Epoxy Composites", PhD Thesis, Rensselaer Polytechnic Institute, Troy, N.Y., 1969.

8. Baker, A. A.: "Carbon Fiber Reinforced Metals - A Review of Current Technology", Materials Science and Engineering, 17, 177, 1975.

9. Darken, L. S., and R. W. Gurry: Physical Chemistry of Metals, McGraw Hill, 363, 1953.

10. Galasso, F. S., and J. Pinto: "Oxidation of Carbon and Metal-Coated Fibers", Fiber Science and Technology, 2, 303, 1970.

11. Braddick, D. M., P. W. Jackson, and P. J. Walker: "Some Mechanical Property and Fracture Studies of Carbon Fiber-Nickel Composites", J. Mat. Sci., 6, 419, 1971.

12. Jackson, P. W., and J. R. Marjoram: "Compatibility Studies of Carbon Fibers with Nickel and Cobalt", J. Mat. Sci., 5, 9, 1970.

13. Sarian, S.: "Elevated Temperature Stability of Carbon Fiber, Nickel Matrix Composites: Morphological and Mechanical Property Degradation", J. Mat. Sci., 8, 251, 1973.

14. Shiota, I., and O. Watanabe: "On the Compatibility of Carbon Fibers in Nickel", Intl. Conf. on Composite Materials, Geneva, 1974.

15. Warren, R., G. H. Anderson, and M. Carlsson: "High Temperature Compatibility of Carbon Fibers with Nickel," J. Mat. Sci., 13, 178, 1978.

16. Barclay, R. B., and W. Boorfield: "Carbon Fiber/Nickel Compatibility", J. Mat Sci., 6, 1076, 1971.

17. Kistler, C. W., and D. E. Niesz: AD854149, P164316(7), 1969.

18. Rashid, M. S., and C. D. Wiskus: "Development of Carbide Coatings for Graphite Filaments", Ceramic Bulletin, Vol. 51, No. 11, 836, 1972.

19. Zabolotskii, A. A., S. E. Salibekov, I. A. Kantsevich, N. P. Ignatova, and A. I. Chesnyak: "Reaction Between Carbon Fibers and Nickel Through a Zirconium Nitride or Titanium Carbide Diffusion Barrier", Soviet Powder Metallurgy and Metal Ceramics, Vol. 16, No. 7, 519, 1977.

20. Shorshorov, M. Kh., L. M. Ustinov, A. M. Zirlin, V. I. Olefirenki, and L. V. Vinogradov: "Brittle Interface Layers and The Tensile Strength of Metal Matrix-Fiber Composites", J. Mat. Sci., 14, 1850, 1979.

21. Weibull, W.: "A Statistical Theory of the Strength of Materials", Ing. Vetenskaps Acad. Hande (Royle Swedish Inst. Engineering Research Proceedings), No. 151, 1939.

22. Koppenaal, T., and N. Parikh: "Fiber-Reinforced Metals and Alloys", ARF 2221-3, Armour Res. Foundation, Chicago, Illinois, 1961.

23. Sara, R. V.: "Fabrication and Properties of Graphite - Fiber, Nickel-Matrix Composites", Society of Aerospace Material and Progress Engineers, 14th National Symposium & Exhibit, Cocoa Beach, Fla., II-4A-4, Nov. 1968.

24. Naidich, Y. V., and G. A. Kolesnichenko: Porosh. Met. SSR, Vol. 1, No. 6, 55, 1961.

25. Schmidt, D., and R. Hellman: U. S. Patent 3,462,288, 1969.

26. LaIaconna, F. P.: "Graphite Aluminum Composites", NASA Marshall Space Flight Center, unpublished work, 1971.

27. Davis, L. W., and S. Bradstreet: "Metal and Ceramic Matrix Composites", Cahners Pub. Co., Boston, Massachusetts, 1970.

28. DeLamotte, E., K. Phillips, A. J. Perry, and H. R. Killias: "Continuously Cast Aluminum-Carbon Fiber Composites and Their Tensile Properties", J. Mat. Sci., 7, 346, 1972.

29. Pepper, R. T., and E. G. Kendall: "Metal Impregnated Graphite Fibers and Methods of Making Same," U. S. Patent No. 3,770,488.

30. Kendall, E. G., and W. C. Harrigan: "New Fiber Reinforcement for Graphite-Aluminum Composites", Aerospace Report, No. ATR-77 (8162)-2, 1977.

31. Hertzberg, R. W., and J. A. Ford, United Aircraft Corp. Rept. B-9160068-1,2 (1963).

32. Hertzberg, R. W., F. D. Lemkey, and J. A. Ford: "Mechanical Behavior of Lamellar (Al-$CuAl_2$) and Wisker Type (Al-Al_3Ni) Undirectionally-Solidified Eutectic Alloys", Transactions AIME, Vol. 233, 342, 1965.

33. Verhoeven, J. D., and R. H. Homer: "The Growth of Off-Eutectic Composites from Stirred Melts", Met. Soc. of AIME Transactions, Vol. 1, 3437, 1970.

34. Baker, A., A. Martin, and R. Bache: "Carbon-Fiber/Metal-Matrix Composites: Fabrication by Electrodeposition", Composites, 2, 154, 1971.

35. Goddard, D. M., W. C. Harrigan, Jr., and D. L. Dull: "Fiber Reinforced Lead Composites: Their Preparation and Potential Applications", Aerospace Corp. Report No. ATR-78(8162)-2, 1977.

36. Kendall, E. G.: "Metallic Matrix Composites", Composite Materials, Vol. 4, Ed. by K. G. Kreider, Academic Press, 1974.

37. Riley, W. C.: "Graphite", High Temperature Materials and Technology, Wiley, 1967.

38. Orowan, E.: "Fatigue and Fracture of Metals", Symposium at Massachusetts Institute of Technology, John Wiley and Sons., Inc., New York, 1950.

39. Brophy, J. H., H. W. Hayden, and J. Wulff: "Sintering and Strength of Coated and Co-Reduced Nickel Tungsten Powder", Transactions AIME, 221, 1225, 1961.

40. Schiff, D.: "Pyrolytic Materials for Re-entry Applications", Metals Engineering Quarterly, American Society of Metals, 32-42, Nov. 1962.

41. Eremenko, V. N., Ya. V. Natanzon, and V. P. Titov: "Dissolution Kinetics and Diffusion Coefficients of Iron, Cobalt and Nickel in Molten Aluminum", Soviet Materials Science Journal, Vol. 14, No. 6, 3, 1978.

42. Rieck, G. D., M. M. P. Janssen: "Reaction Diffusion and Kirkendall-Effect in the Nickel-Aluminum System," Transactions AIME, Vol. 239, 1, 372, September 1967.

43. Hansen, M.: "Construction of Binary Alloys," Metallurgy and Metallurgical Engineering Series, McGraw Hill Book Company, Inc., 1958.

44. Jech, R. W., D. L. McDaniels, and J. W. Weeton: "Metals Reinforced with Fibers," Metal Progress, Vol. 78, No. 6, 118, 1960.

45. Coleman, B. D.: "The Strength of Classical Fibers and Fiber Bundles," J. Mech. Phys. Solids, 7, 60-70, 1958.

46. Sadowsky, M. A., and E. Sternberg: "Stress Concentration Around a Tri-Axial Ellipsoidal Cavity," Journal of Applied Mechanics, 71, 149, 1949.

47. Kelly, A. and G. Davies: Metallurgical Reviews, 10, No. 37, 1965.

48. LeRoy, W. and P. G. Sullivan: "Exploratory Development of Graphite-Aluminum Composites, Nevada Engineering and Technology Corp. Report No. 5334-3, October 1977.

APPENDIX

TABLE I

COMPARISON OF SOME OF THE PROPERTIES
AND THE COST OF VARIOUS FIBERS

Fiber Type Commercially Available	σ_{uts} ksi	E msi	Density gm/cc	Cost per/lb.
Boron	475	58-60	2.60	$220
PRD-49	400	20	1.47	$ 50
Carbon: i, High Strength	400	30-34	1.73	$ 40
ii, High Modulus	420	56-58	1.90	$100
Glass	500	10.5	2.54	$ 60

TABLE II

PROPERTIES OF COMMERCIALLY AVAILABLE GRAPHITE FIBERS

Trade Name	Grade	Precursor*	Tensile Strength ksi	E msi	ρ gm/cc	Form
Union Carbide (Thornel)	T-25	R	180	25	1.43	2-Ply Yarn
	T-40	R	250	40	1.56	2-Ply Yarn
	T-50	R	300	50	1.65	2-Ply Yarn
	T-75	R	365	75	1.82	2-Ply Yarn
	T-400	P	450	30	1.78	1-Ply Yarn
Hilco	HMG-25	R	150	25	1.5	Yarn
	HMG-40	R	250	40	1.7	Yarn
	HMG-50	R	300	50	1.8	Yarn
Celanese (Celion)	GY-70	P	300	75	1.9	--
Hercules/Courtaulds	A	P	390	31	1.8	10,000 tow
(Grafil)	HM	P	300	55	1.88	10,000 tow
(Magnamite)	HT	P	350	40	1.72	10,000 tow
Great Lakes (Fortifil)	3-T	P	250	28	1.76	150,000 tow
	4-T	P	350	37	1.78	50,000 tow
	5-T	P	400	48	1.79	40,000 tow
	6-T	P	420	59	1.9	50,000 tow
Whittaker/Morganite (Modmor)	I	P	250	60	2.0	10,000 tow
	II	P	400	40	1.76	10,000 tow

*R = Rayon; P = Polyacrylonitrile. (Source: Manufacturer's Literature)

TABLE III

SOME OF THE ADVANTAGES AND DISADVANTAGES OF A METAL MATRIX COMPARED WITH A RESIN MATRIX

Advantages	Disadvantages
• Increased Temperature Capability	• Increased Density
• Reduced Elastic Anisotropy	• Chemically Reactive
• Increased Buckling Stability	• Limited Corrosion Resistance
• Increased Electrical and Thermal Conductivity	
• Normally Non-combustible	
• Increased Erosion Resistance	
• Low Vapor Pressure	
• Resistant to Ultraviolet Radiation	
• Dimensional Stability in Wet Conditions	

TABLE IV

MECHANICAL AND PHYSICAL PROPERTIES OF AS-CAST GRAPHITE METAL COMPOSITES

Specimen No.	ρ gm/cc	Theoretical ρ gm/cc	Volume Percent of Fibers	Theoretically Calculated Volume Percent of Fibers	σ_{uts} ksi	ROM σ_{uts} ksi	E msi	ROM E msi
Fort 3-7075 Al								
1	2.79	2.92	12.00	12.79	17.10	47.09	12.55	12.4
2	2.95	3.13	15.00	15.98	21.78	53.5	14.07	13.00
3	2.97	3.20	19.00	19.18	21.97	65.1	15.17	13.90
4	--	3.40	22.00	25.57	29.11	74.8	18.127	15.4
Fort 5-7075 Al								
1	2.85	2.94	13.0	12.95	13.20	40.46	12.86	13.82
2	3.35	3.53	33.33	36.27	8.9	95.32	---	22.66
Fort 3 - Zn								
1	5.93	6.59	12.5	12.79	23.73	45.37	12.28	14.25
2	6.16	6.49	14.96	15.98	45.67	52.53	18.12	14.69
Fort 5 - Zn								
1	6.56	6.69	11.8	10.9	35.27	37.01	12.92	15.92
2	6.50	6.57	12.62	12.59	43.16	41.43	22.41	16.54

TABLE IV (Continued)

Specimen No.	σ gm/cc	Theoretical σ gm/cc	Volume Percent of Fibers	Theoretically Calculated Volume Percent of Fibers	σ_{uts} ksi	ROM σ_{uts} ksi	E msi	ROM E msi
Fort 3 - Pb								
1	8.79	9.99	12.12	12.79	14.84	33.8	4.23	5.39
2	7.88	8.82	22.3	25.57	32.92	60.71	7.95	2.24
Fort 5 - Pb								
1	9.66	10.17	10.96	10.9	23.34	30.09	6.02	7.04
2	7.91	9.09	20.89	20.15	35.17	55.73	10.40	11.60
3	7.18	7.98	31.25	30.22	67.11	82.48	15.54	15.90

TABLE V

PERCENT VOIDS IN COMPOSITE

Specimen	Volume Percent of Fibers	Experimentally Measured ρ gm/cc	Theoretically Calculated ρ gm/cc	Percent Voids in the Composite Specimen
Fort 5-7075 Al				
1	13.00	2.85	2.94	3.06
2	33.33	3.35	3.53	5.09
Fort 3-7075 Al				
1	12.00	2.79	2.92	4.45
2	15.00	2.95	3.13	5.75
3	19.00	2.97	3.20	7.18
4	22.00	--	3.40	--
Fort 3 - Zn				
1	12.5	5.93	6.59	10.01
2	14.96	6.16	6.49	5.08
Fort 5 - Zn				
1	11.8	6.56	6.69	1.94
2	12.62	6.50	6.57	1.06
Fort 3 - Pb				
1	12.12	8.79	9.99	12.01
2	22.3	7.88	8.82	10.65
Fort 5 - Pb				
1	10.96	9.66	10.17	5.01
2	20.89	7.91	9.09	12.98
3	31.25	7.18	7.98	10.02

TABLE VI

EFFECT OF ZONE TRAVEL RATE ON STRENGTH OF FORTIFIL 5 GRAPHITE-Al_3Ni-Al COMPOSITE

Specimen No.	Volume Percent of Fibers Fort 5	Zone Travel Rate Inch/Hour	σ_{uts} ksi	E msi
1DS	13	10	27.78	14.66
2DS	13	10	37.74	---
3DS	13	10	32.98	---
4DS	26	10	82.60	---
5DS	26	10	87.00	---
6DS	13	14	27.41	14.58
7DS	13	5	21.53	---
8DS	13	27.3	23.64	14.78
9DS	13	9	22.77	15.14
10DS	13	2.5	20.55	---
1	13	---	13.20	12.86
2	13	---	11.51	---
3	13	---	9.98	---

TABLE VII

RANK TEST

Specimen No.	As-Cast	Directionally Solidified
1	9.98 (1)	27.78 (4)
2	11.51 (2)	32.98 (5)
3	13.20 (3)	37.74 (6)
	6	15 r_i
	36	225 r_i^2
	$\sum r_i^2 = 261$	

TABLE VIII

CHI-SQUARE DISTRIBUTION

k	w	k	w
1	3.841	16	26.30
2	5.991	17	27.59
3	7.815	18	28.87
4	9.488	19	30.14
5	11.07	20	31.41
6	12.59	22	33.92
7	14.07	24	36.42
8	15.51	26	38.89
9	16.92	28	41.34
10	18.31	30	43.77
11	19.68	40	55.76
12	21.03	50	67.50
13	22.36	60	79.08
14	23.68	70	90.53
15	25.00	80	101.9

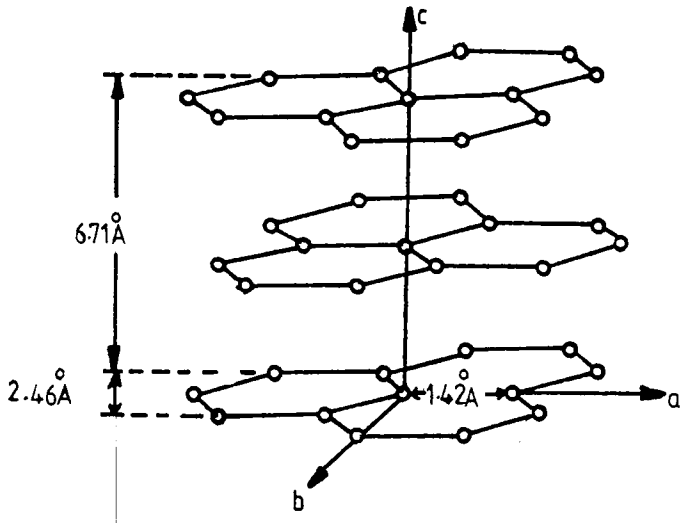


Figure 1. Graphite crystal lattice.

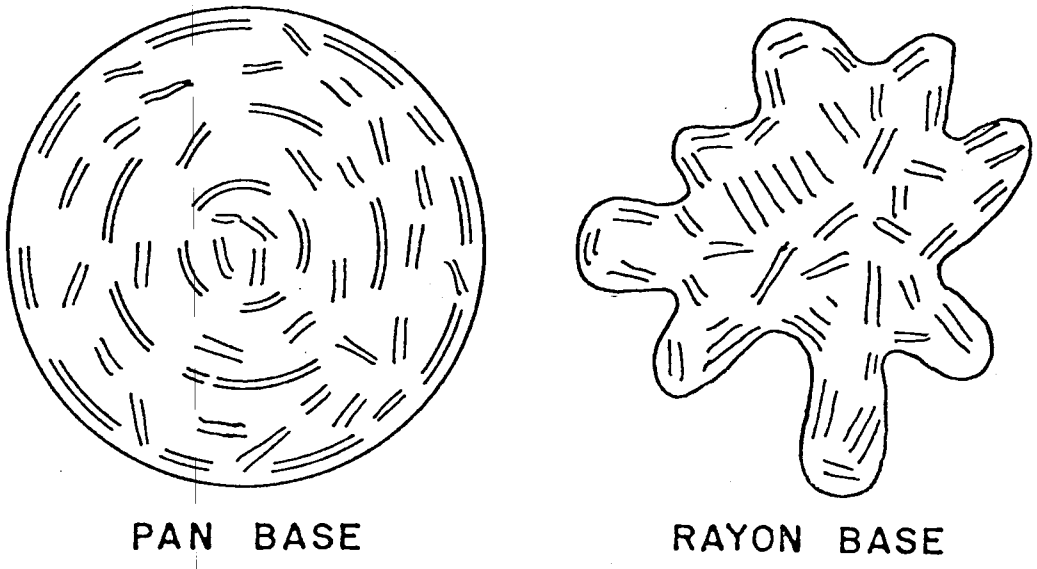
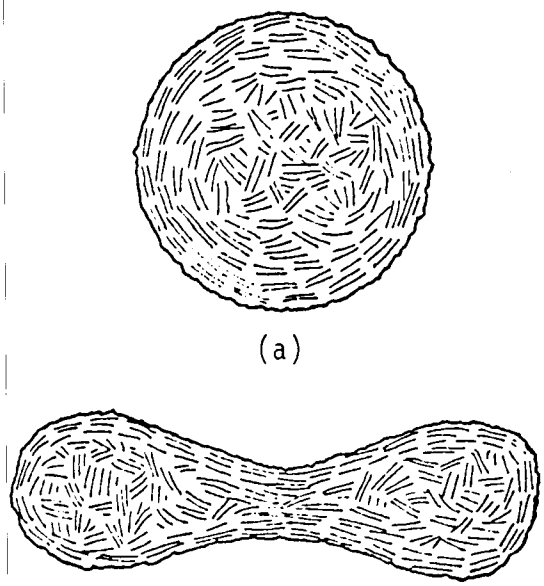


Figure 2. Schematic of observed carbon fiber structures.

Source: LeMaistre, C. W., and R. J. Diefendorf: "The Origin of Structure in Carbon Fibers", Advanced Materials: Composites and Carbon, Amer. Ceramic Soc. Symposium, Chicago, 1971.



(a)

(b)

PAN-based fibers

Figure 3. Schematic diagram of onion-skin model for graphite fibers.

Source: Butler, B. L., and R. J. Diefendorf: "Graphite Filament Structure", Carbon Composite Technology Symposium, 10th Annual, Jan. 1970.

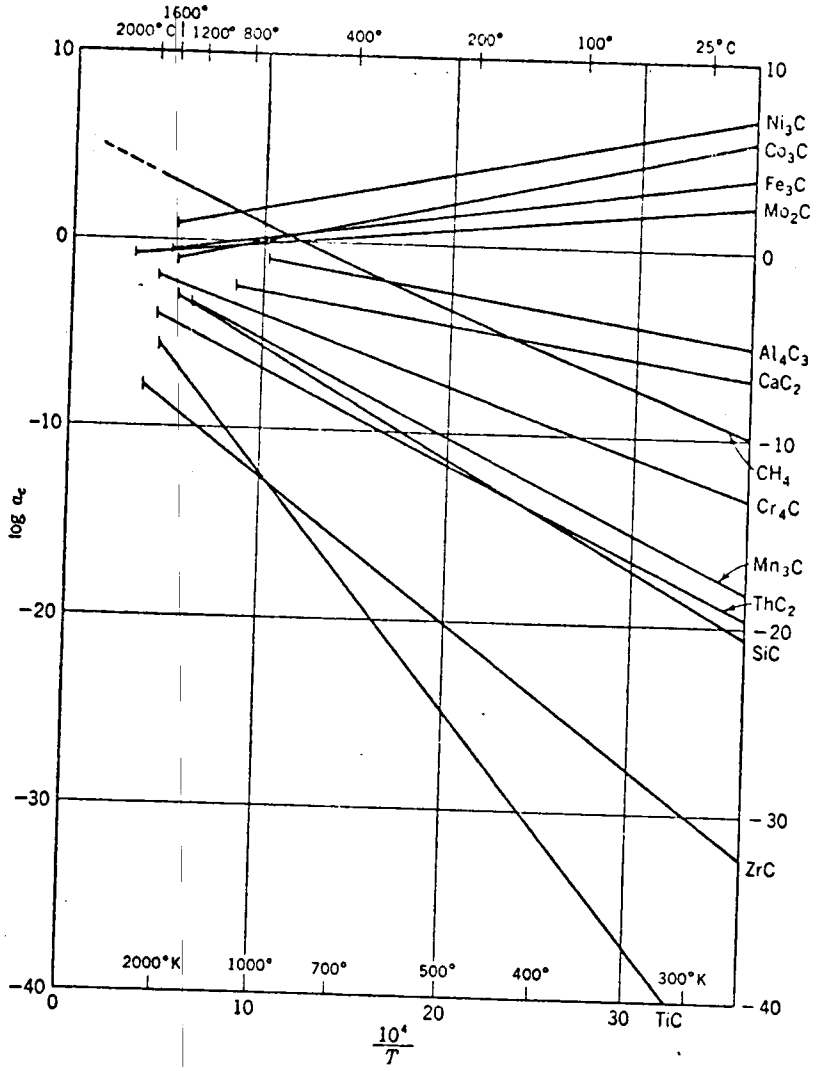
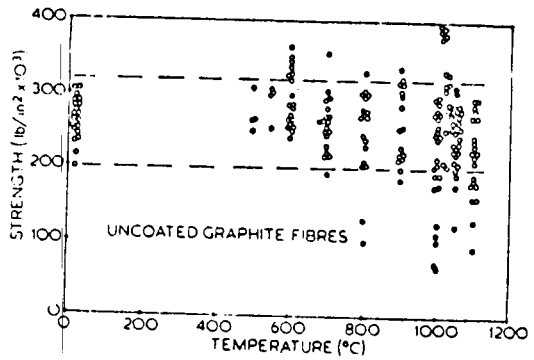
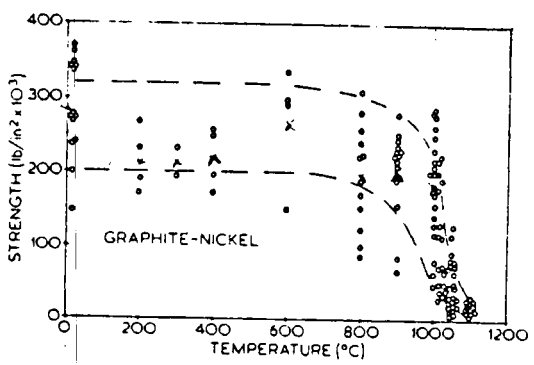


Figure 4. The activity of carbon (standard state = graphite) for several metal-carbide systems as a function of temperature.

Source: Darken, L. S., and R. W. Gurry: Physical Chemistry of Metals, McGraw Hill, 363, 1953.



(a)



(b)

Figure 5. Effect of isothermal exposure of graphite fibers, in vacuum, on the strength (a) uncoated graphite fibers, and (b) nickel-coated graphite fibers.

Source: Jackson, P. W., and J. R. Marjoram: "Compatability Studies of Carbon Fibers with Nickel and Cobalt", J. Mat. Sci., 5, 9, 1970.

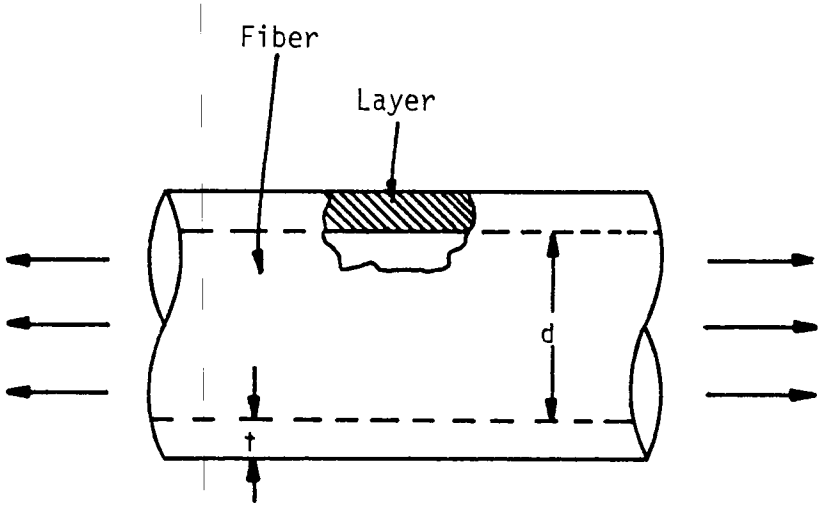


Figure 6. The model system--fiber/layer.

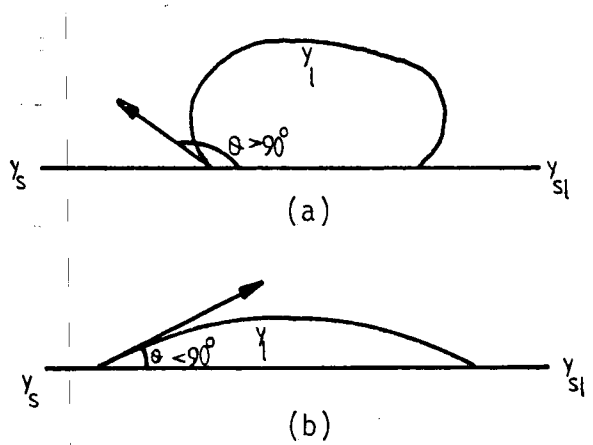


Figure 7. Wetting of graphite by melts. (a) No wetting
(b) Wetting

Source: Naidich, Y. V., and G. A. Kolesnichenko: Porosh. Met. SSR, Vol. 1, No. 6, 55, 1961.

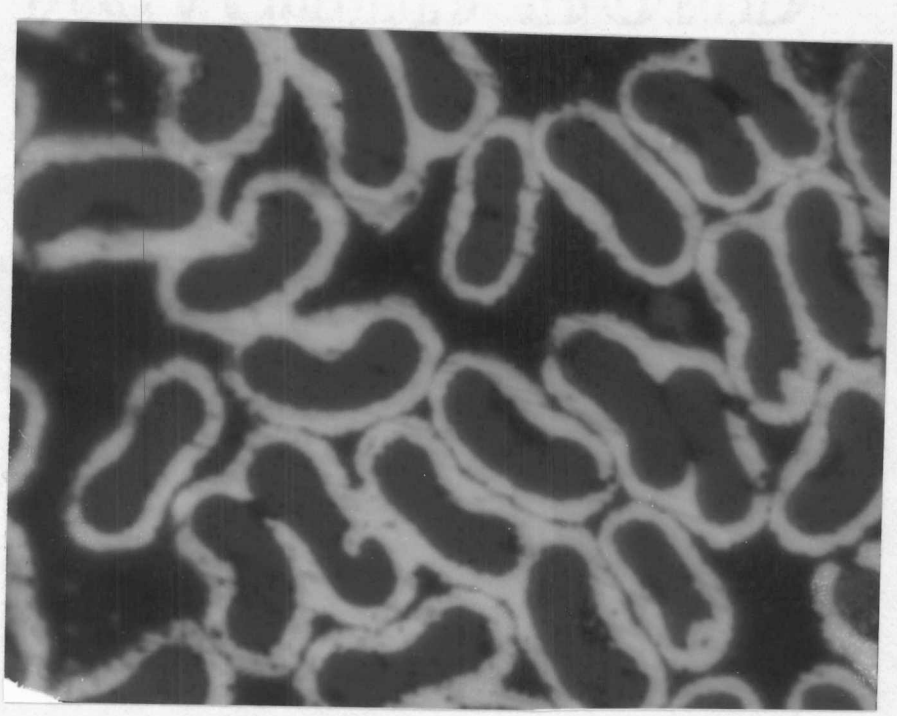


Figure 8. Nickel-coated graphite fibers, 1815X.

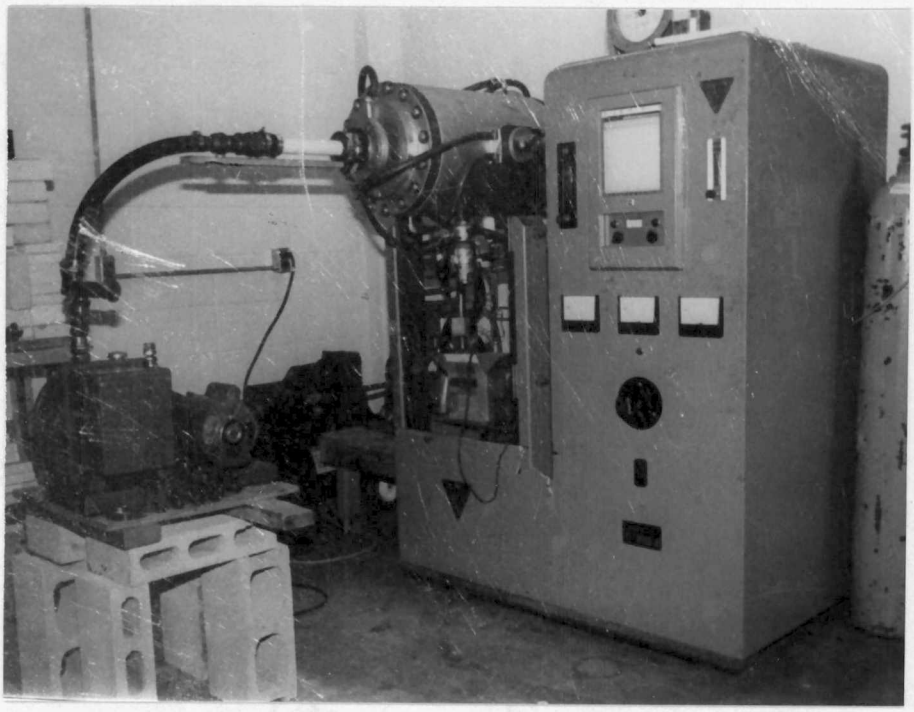


Figure 9. Set-up for heating nickel-coated graphite fibers.

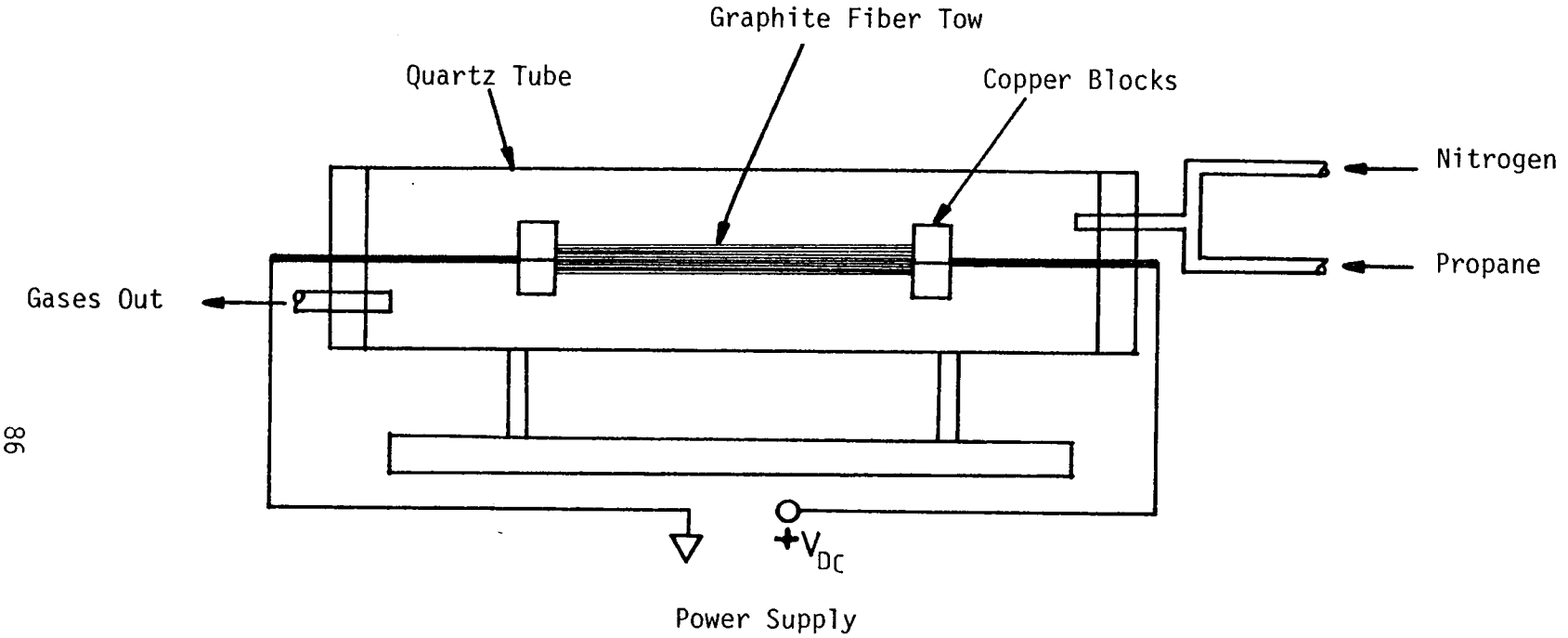


Figure 10. Apparatus to coat pyrolytic carbon on fiber tows.

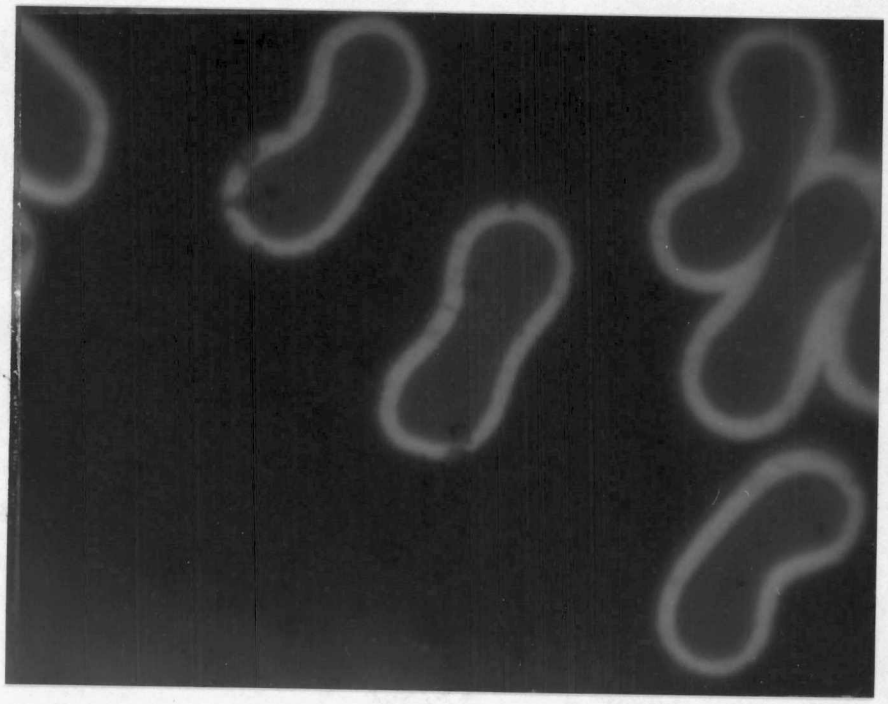


Figure 11. Nickel-coated Fortifil 5 fibers obtained from Great Lakes Carbon Corp., 2200X.

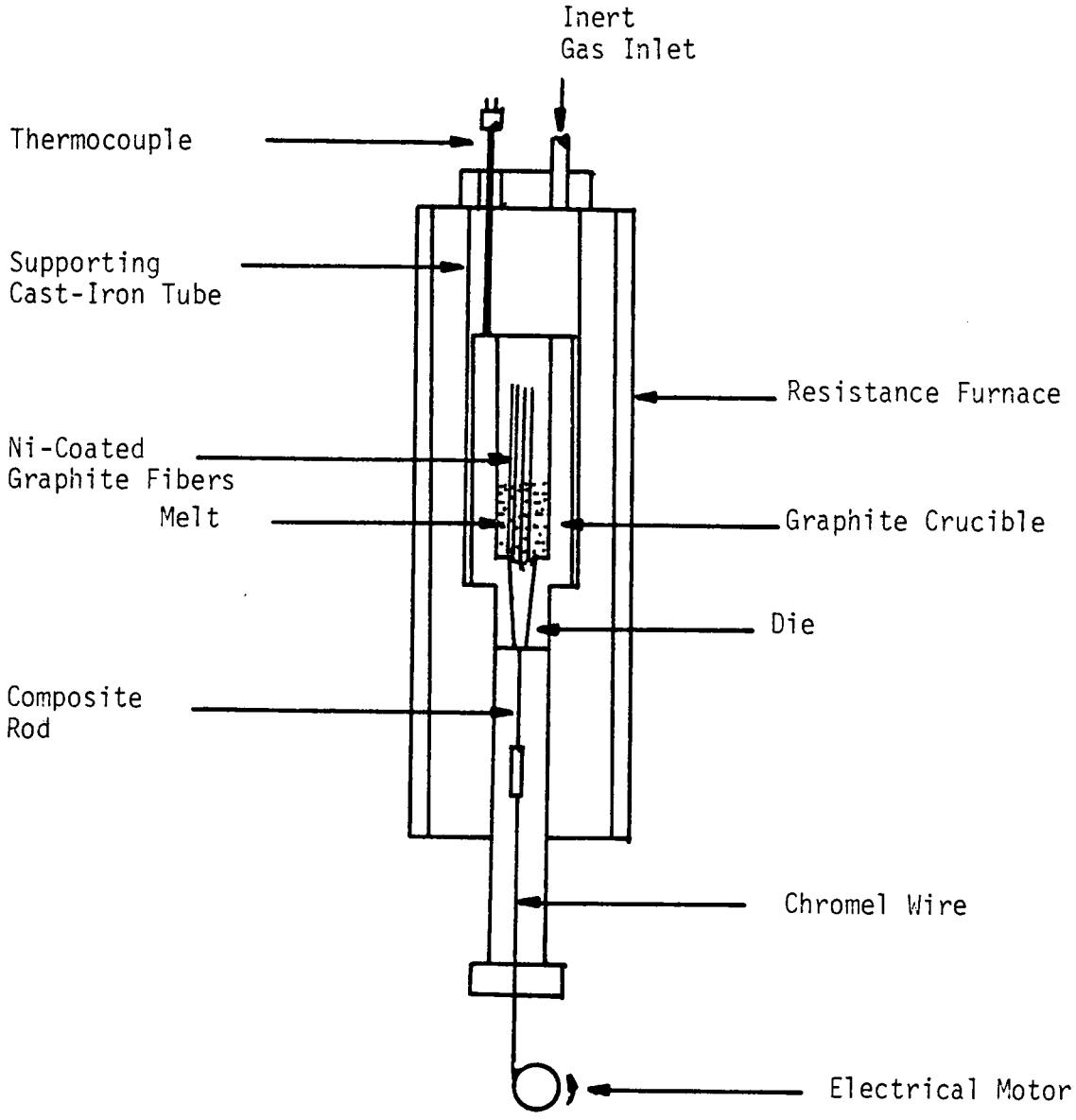


Figure 12. Experimental set-up, to fabricate the composite rods.

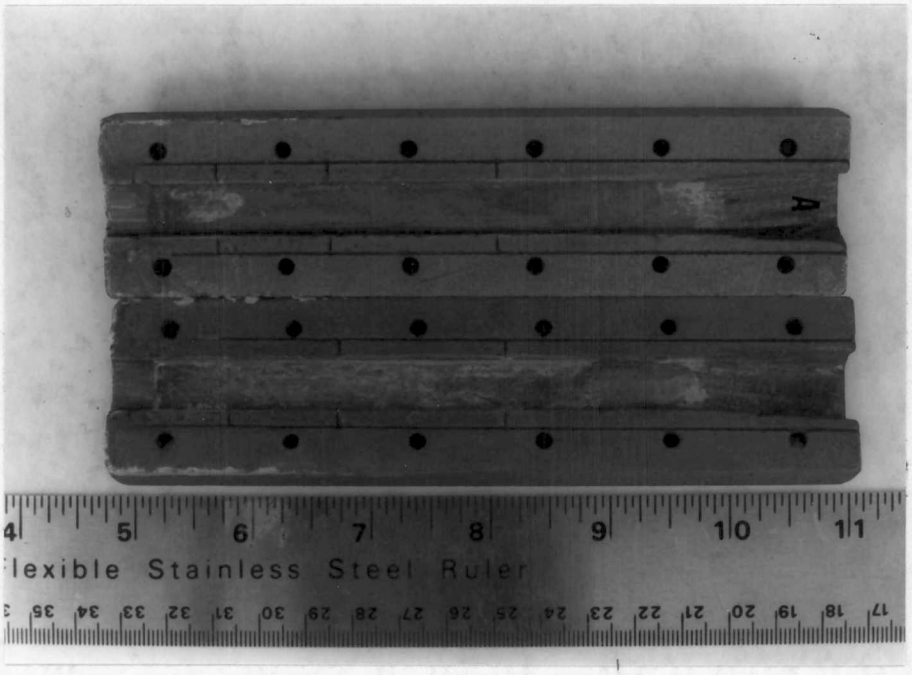


Figure 13. Graphite mold used to fabricate the composites of rectangular shape.

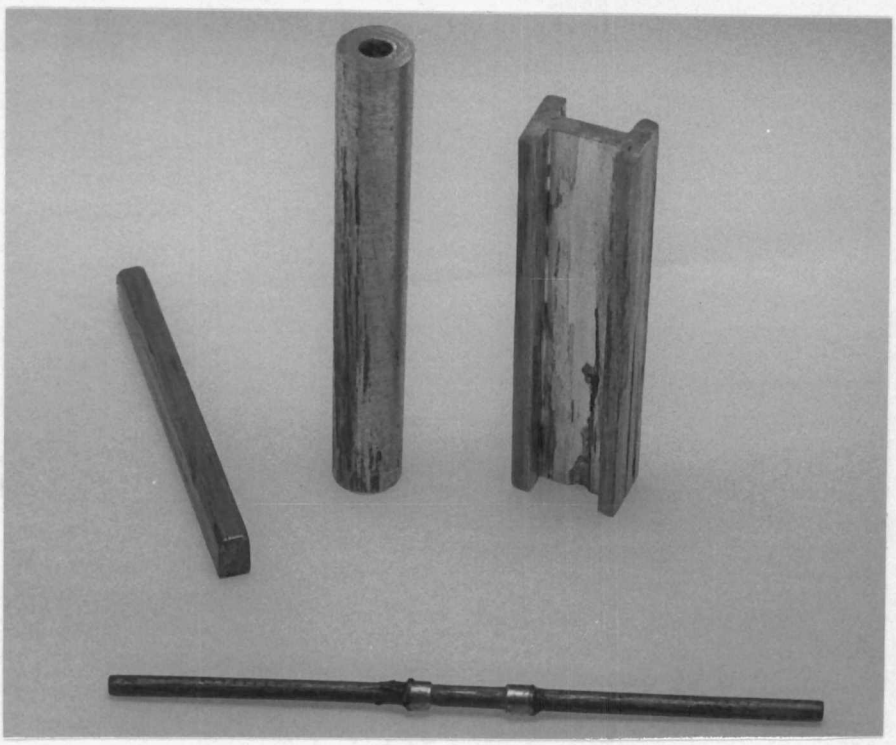


Figure 14. The structural shapes in which the composites can be fabricated.

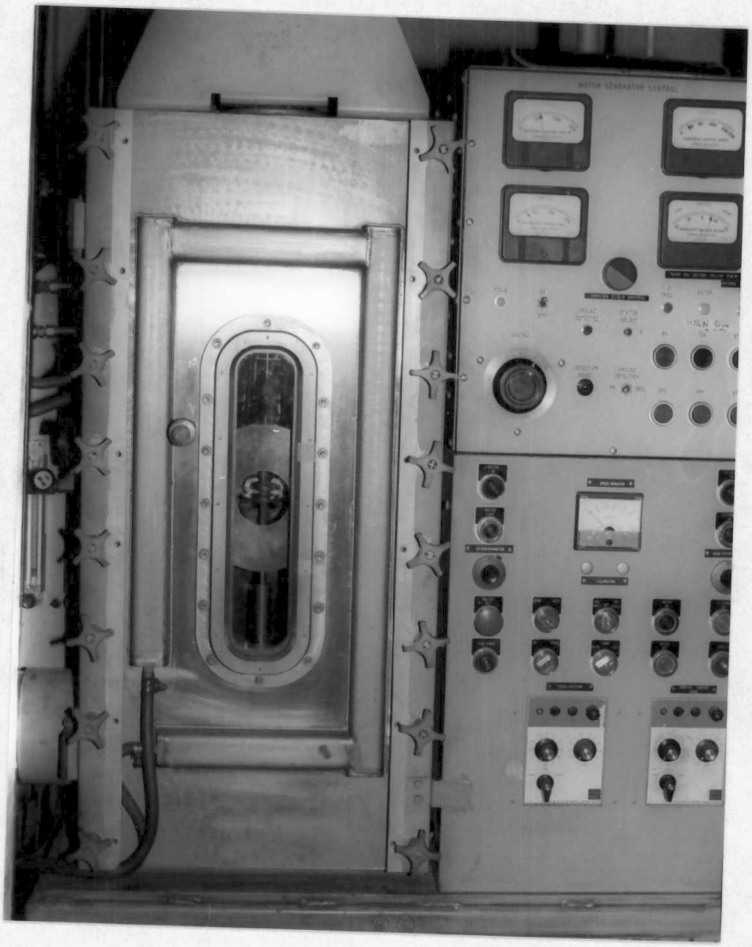


Figure 15. Zone melting unit.

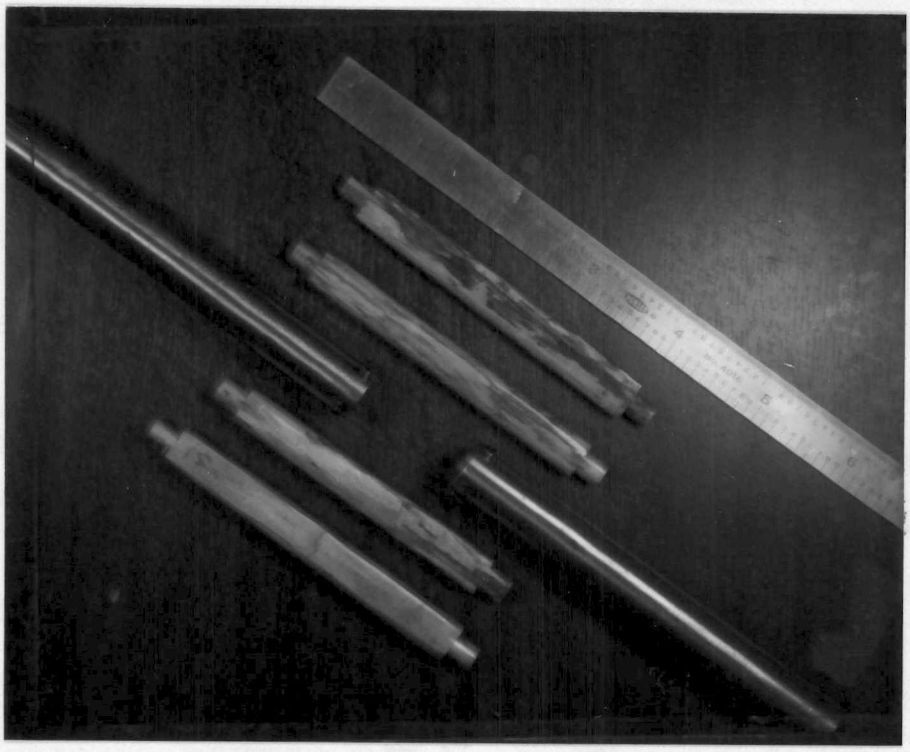


Figure 16. Specimen mount and the graphite-Al composite specimens for directional solidification.

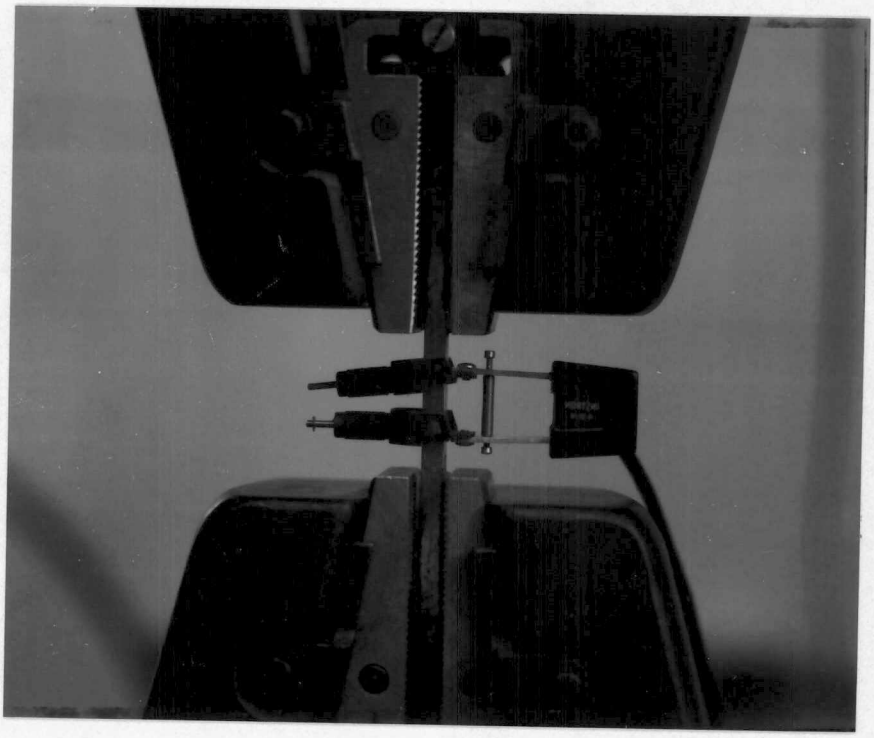


Figure 17. Instrumented test specimen mounted in the tensile machine.

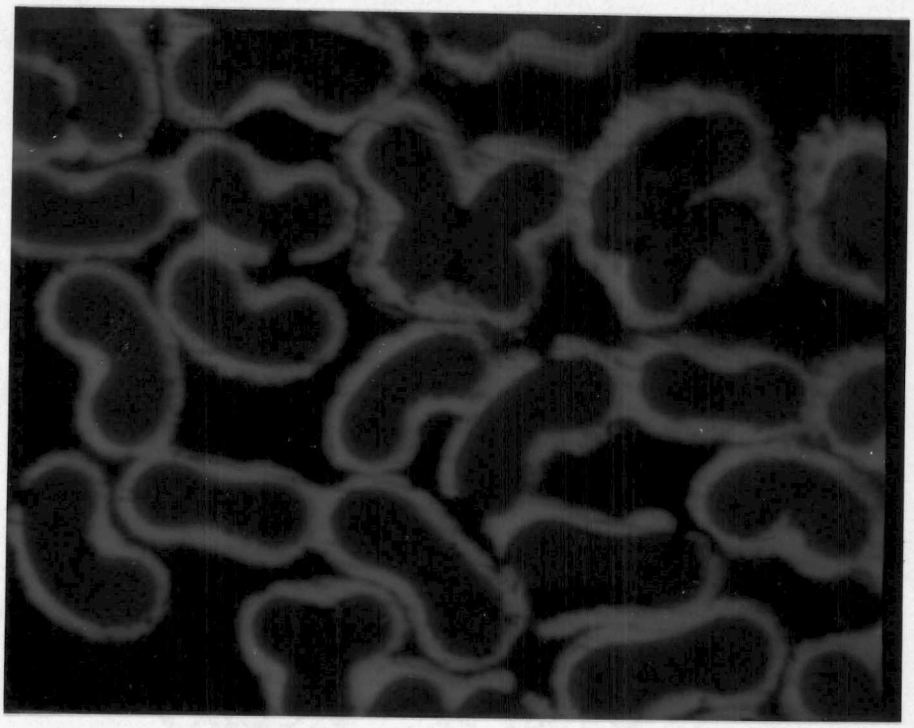


Figure 18. Fortifil 5 graphite fibers Ni-coated and heat-treated at 850° C for two hours.

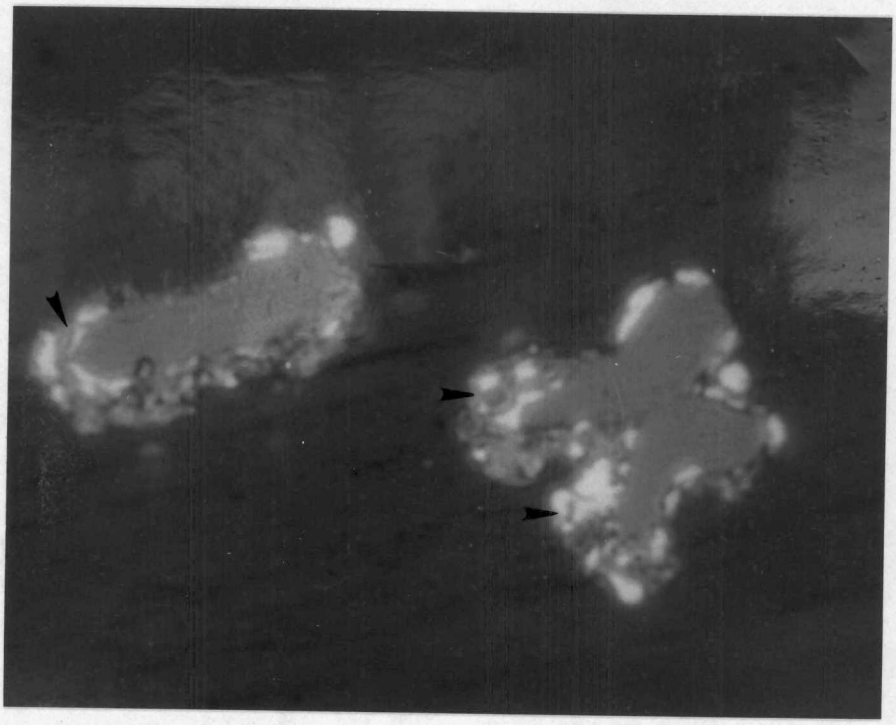


Figure 19. Fortifil 5 PAN-based fibers partially recrystallized by nickel after heating for one hour at 1,000° C.

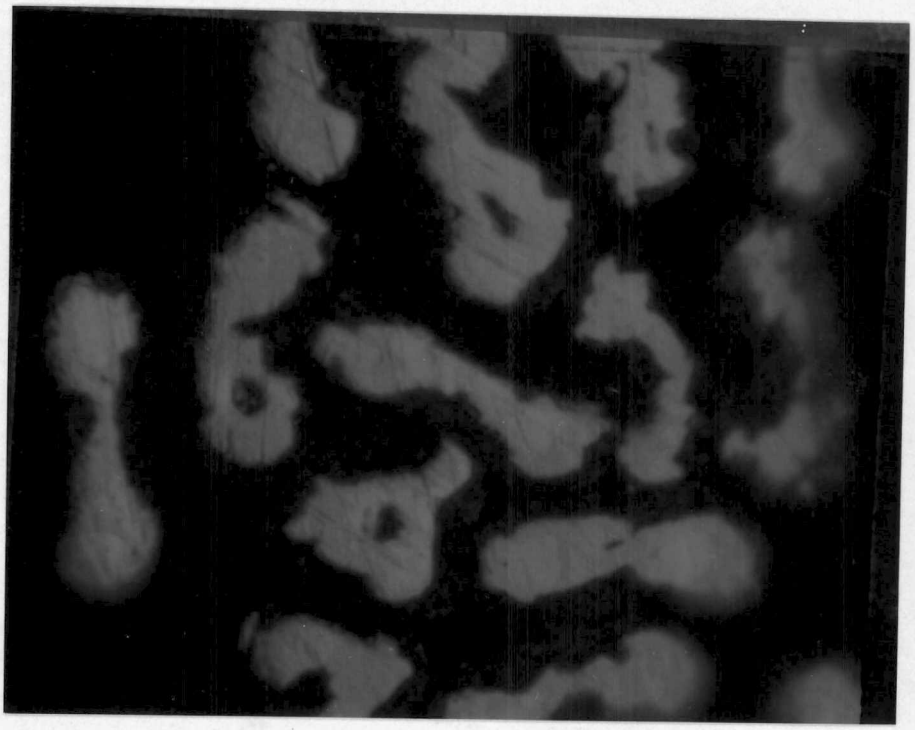


Figure 20. Fortifil 5 PAN-based graphite fibers fully recrystallized by nickel after one hour at 1,100° C.

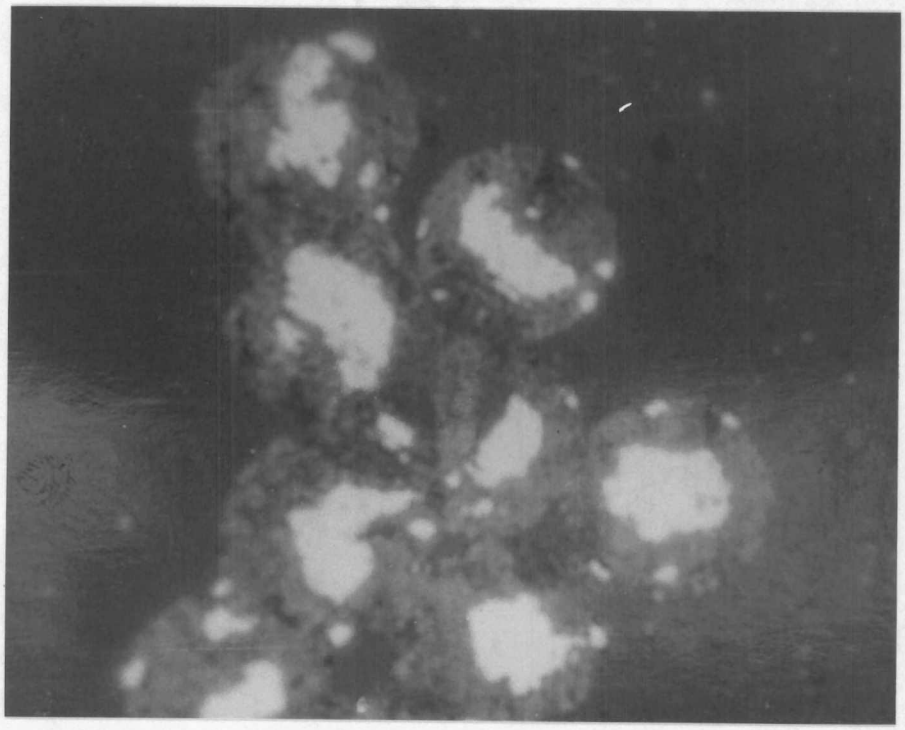


Figure 21. Pitch-based graphite fibers fully recrystallized by nickel after one hour at 1,100° C, 2500X.

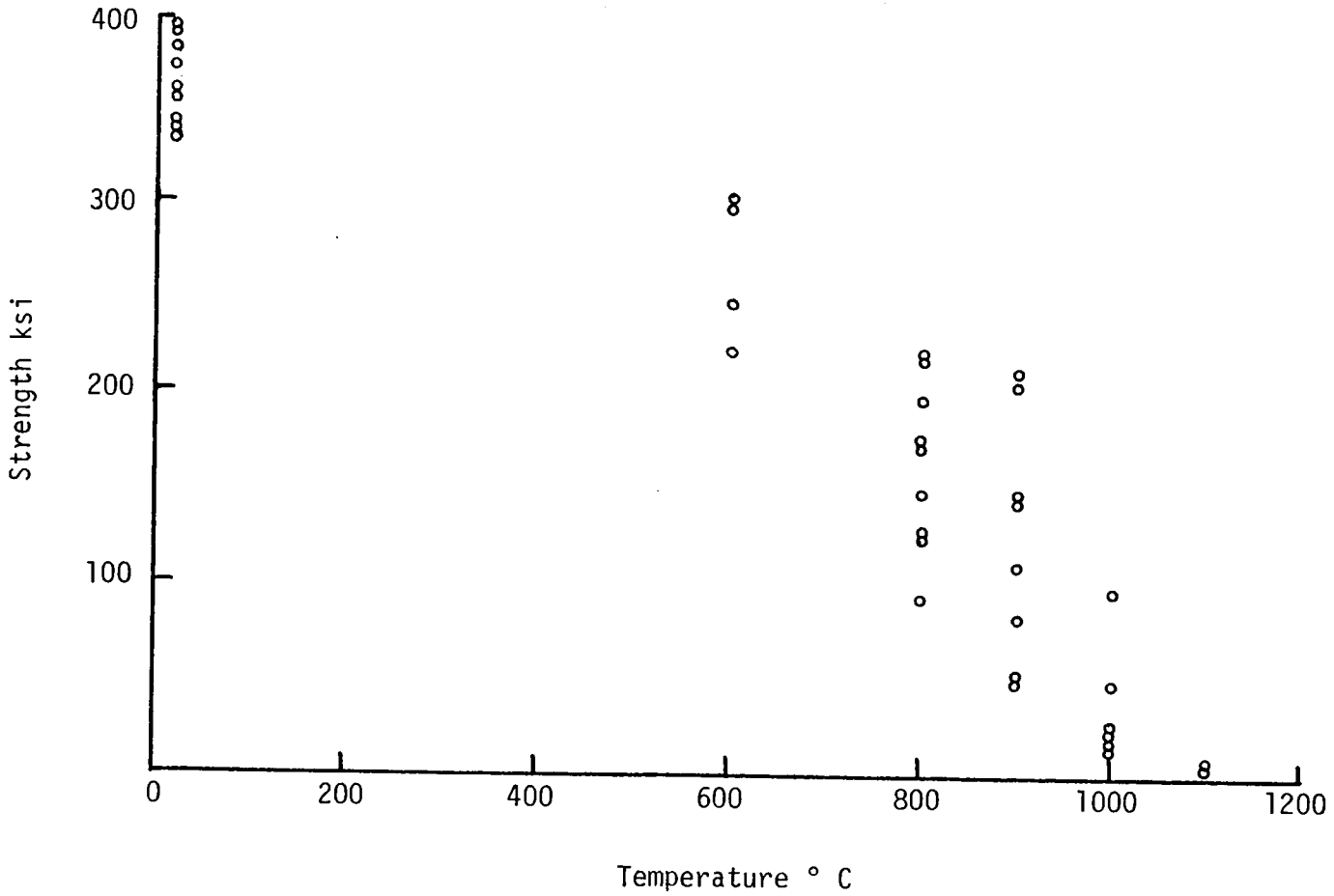


Figure 22. Strength of nickel-coated Fortifil 5 graphite fibers after heating for one hour at various temperatures.



Figure 23. Fortifil 5 graphite fibers oxidized.

Fortifil 5 graphite fibers oxidized (partial vacuum oxidation at 22 mm Hg), Ni-coated and heat-treated at 1,100° C for one hour in vacuum, 1815X.

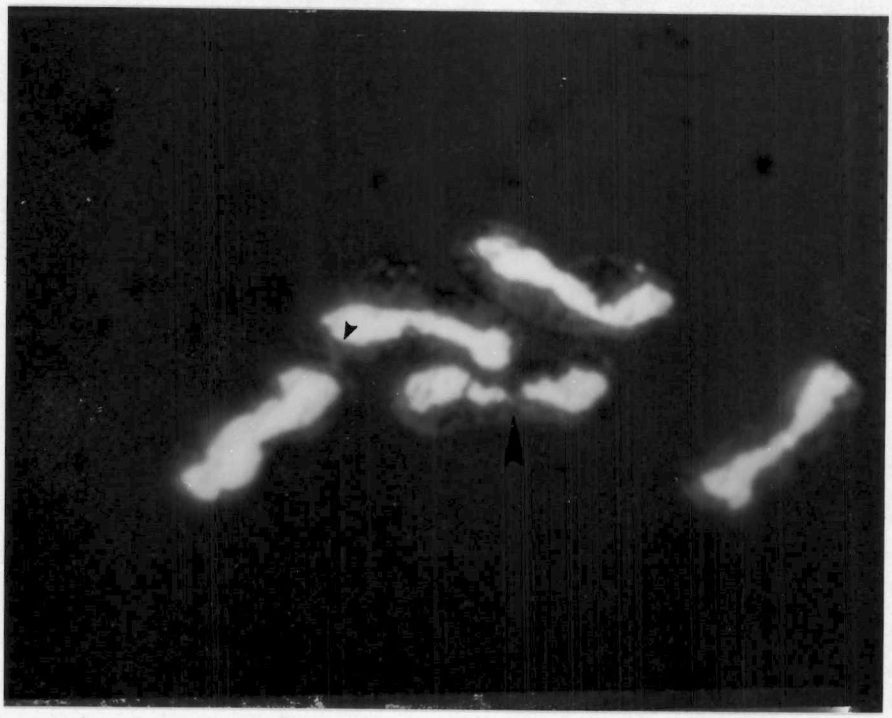


Figure 23. (Continued)

Fortifil 5 graphite fibers oxidized (partial vacuum oxidation at 35 mm Hg pressure), Ni-coated and heat-treated at 1,100° C for one hour in vacuum, 1815X.

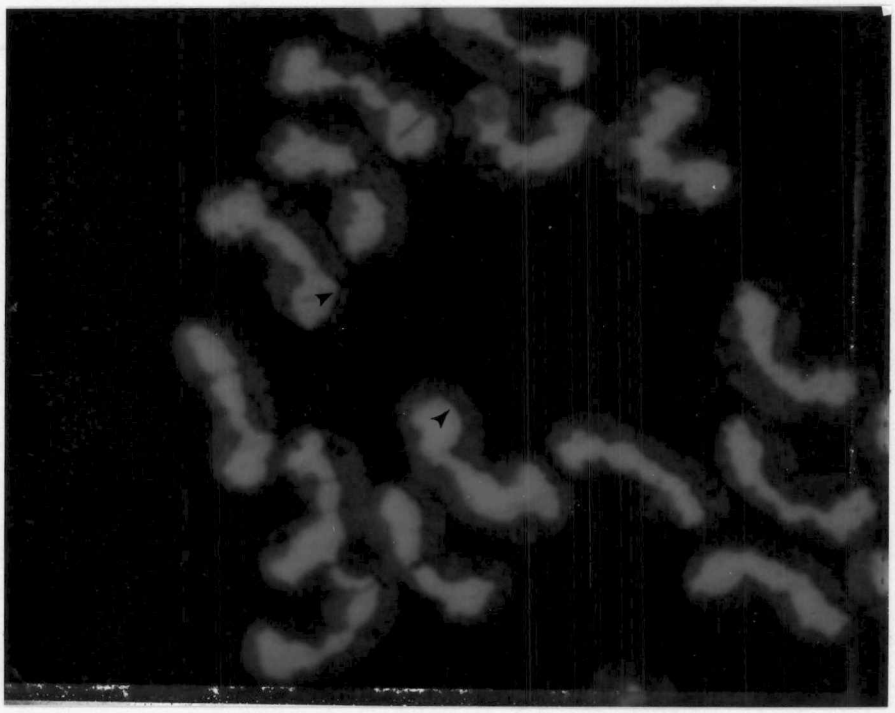


Figure 23. (Continued)

Fortifil 5 graphite fibers oxidized (partial vacuum oxidation at 40 mm Hg pressure), Ni-coated and heat-treated at 1,100° C for one hour in vacuum, 1815X.

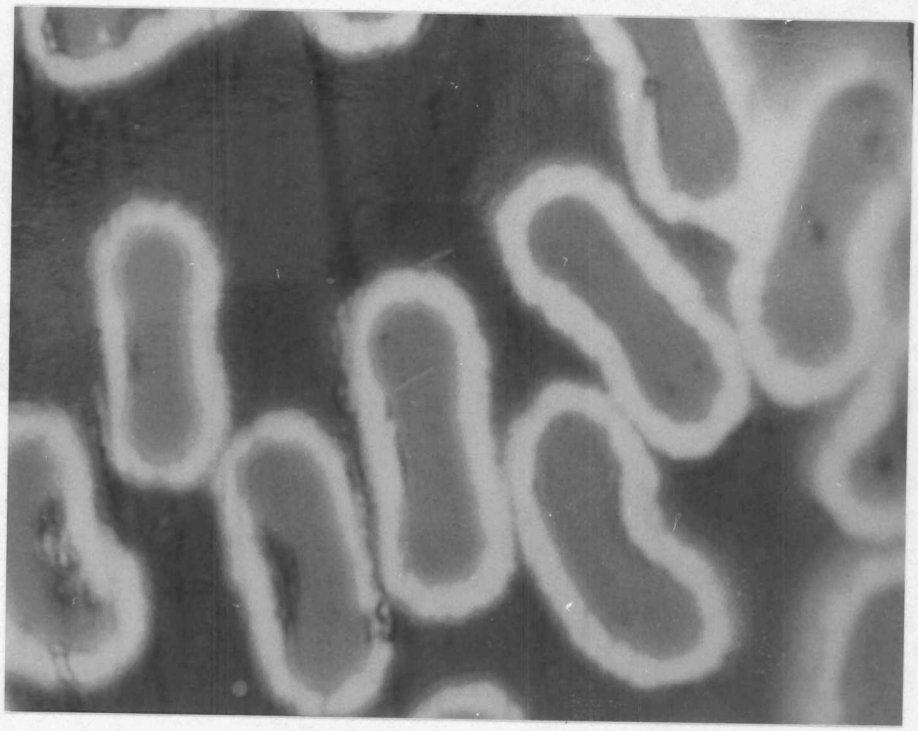


Figure 24. Fortifil 5 PAN-based graphite fibers air-oxidized for one hour at 1,100° C; nickel-plated, and heated one hour at 1,100° C, 2500X.

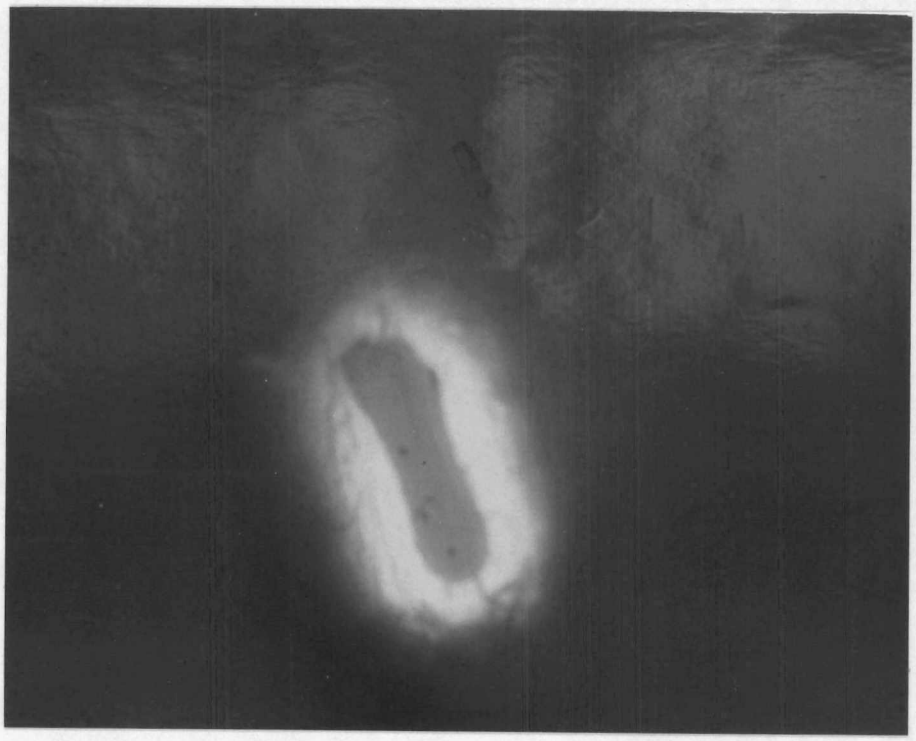


Figure 25. Fortifil 5 PAN-based graphite fiber sputter-coated with carbon, nickel-plated and heated for one hour at 1,100° C, 2500X.

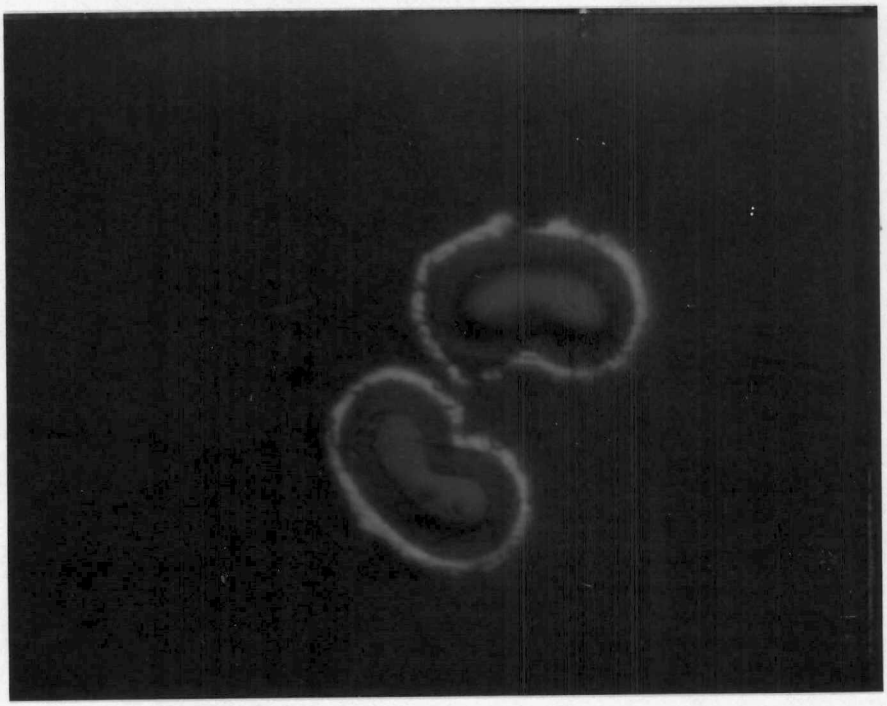


Figure 26. Fortifil 5 fiber Pyrdytic-carbon-coated, nickel-coated and heated at 1,100° C for one hour, 3000X.

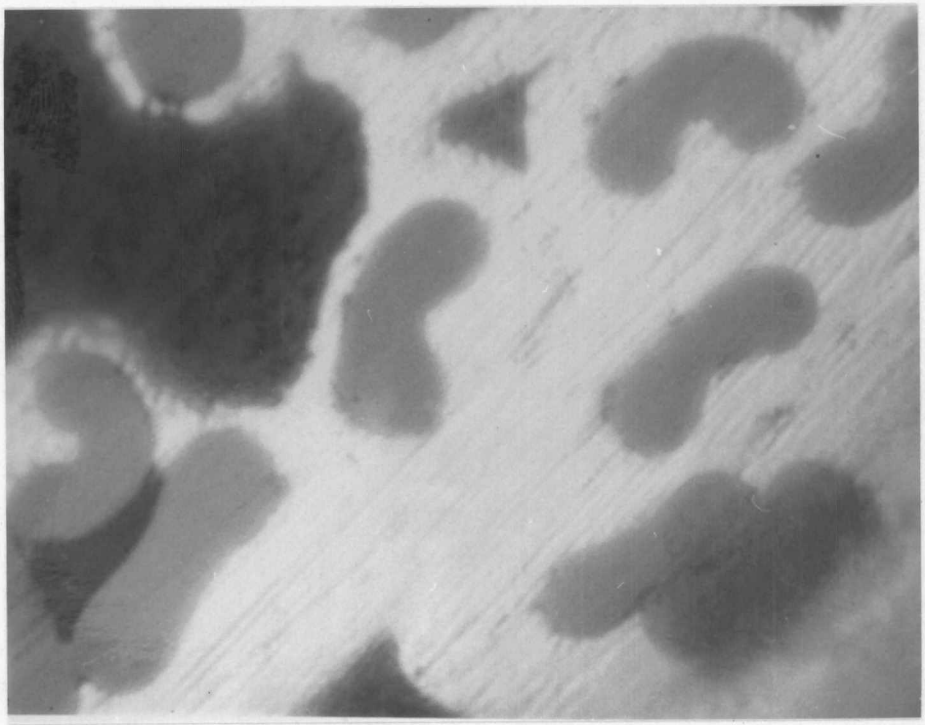


Figure 27. Fortifil 5 PAN-based graphite fibers with carbonized epoxy resin-coating and nickel-plating after one hour, 1,100° C heat treatment, 2500X.

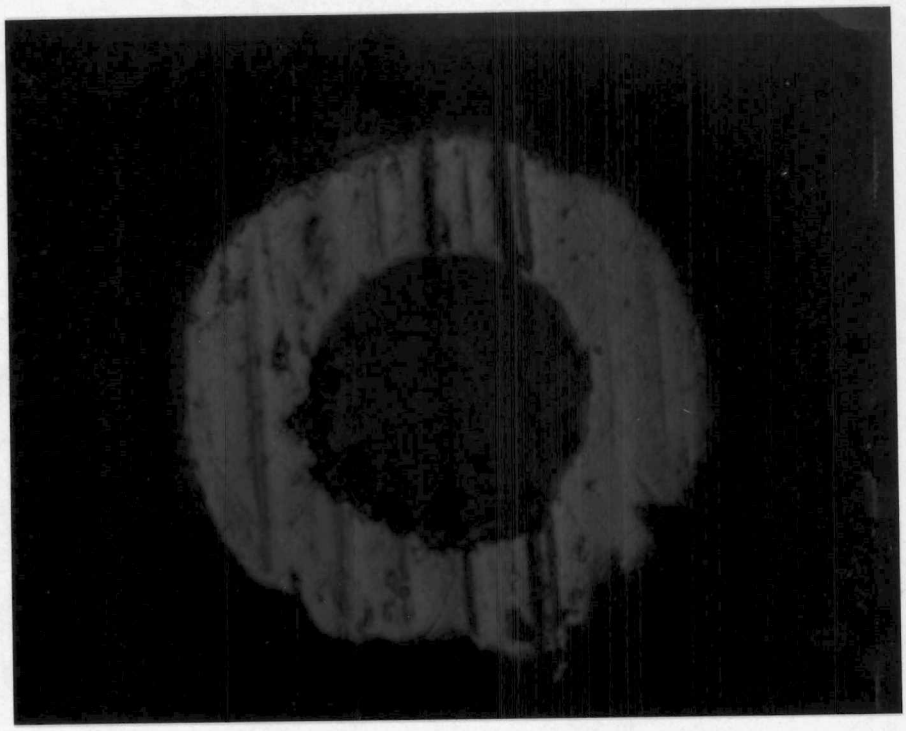


Figure 28. Mono-carbon fiber, coated with pyrolytic carbon (HT 2,700° C, one hour) obtained from AVCO, nickel-coated and heated at 1,100° C for 24 hours, 3000X.

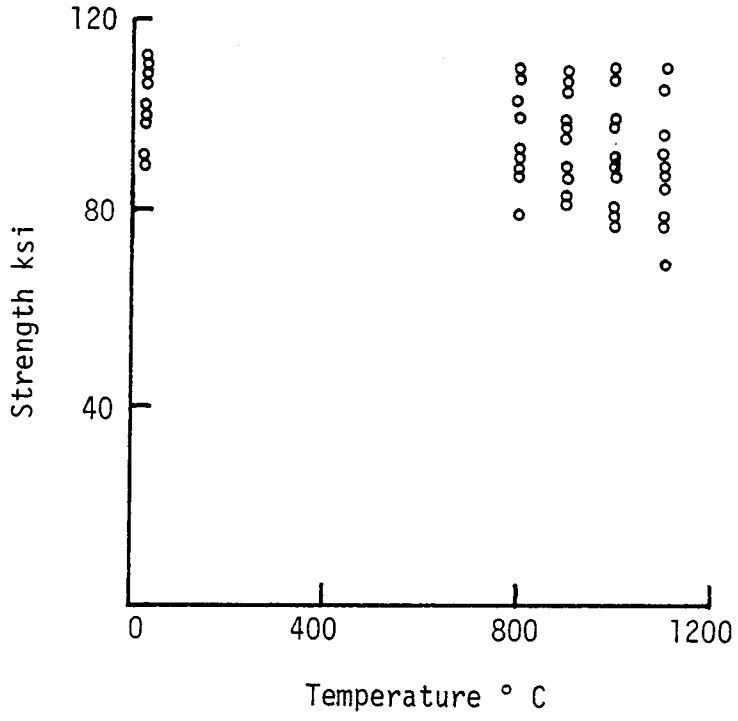


Figure 29. Strength of nickel-coated-AVCO graphite fibers (pyrolytic-coated, heat-treated at 2,700° C for one hour) after heating for two hours at various temperatures.

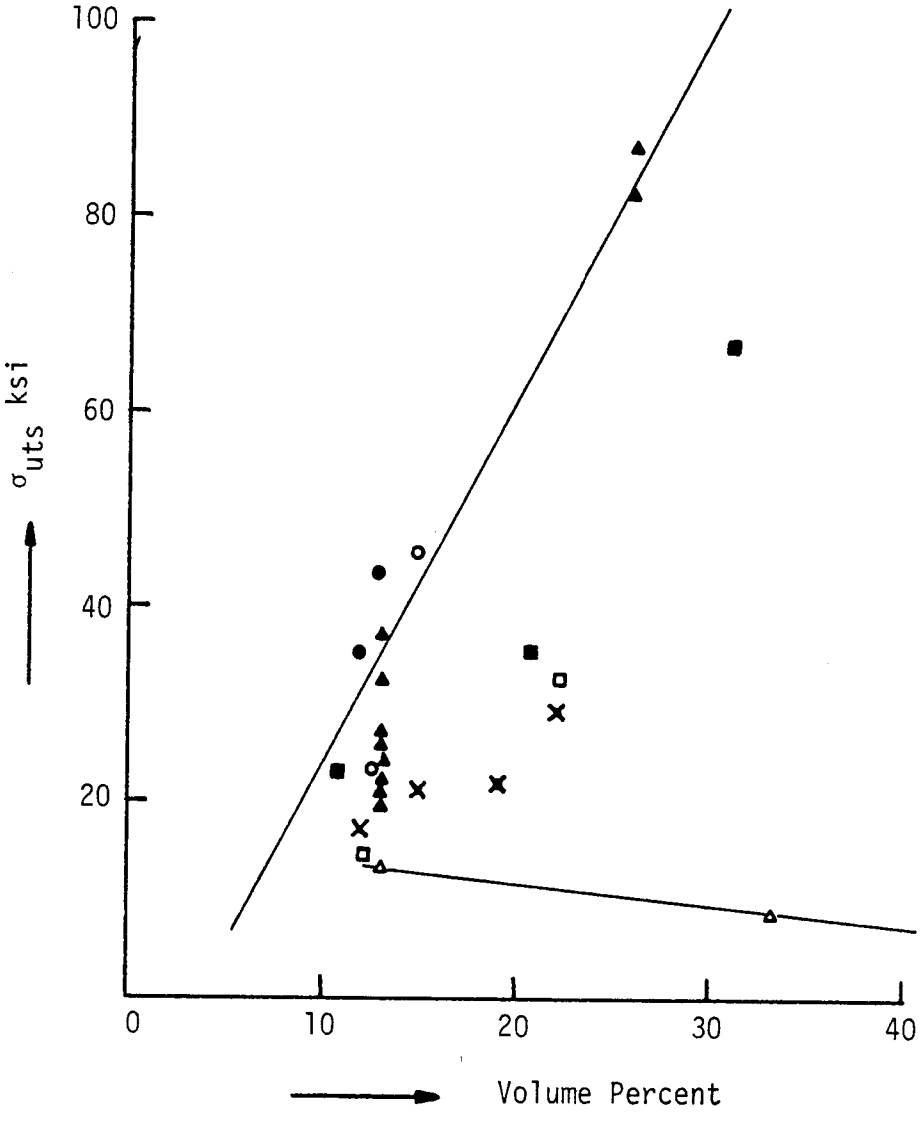


Figure 30. Tensile strength vs. volume percent of fibers plot of various composites (as-cast and after-directional solidification in the case of Al - graphite). (Nomenclature for symbols is listed in Figure 31).

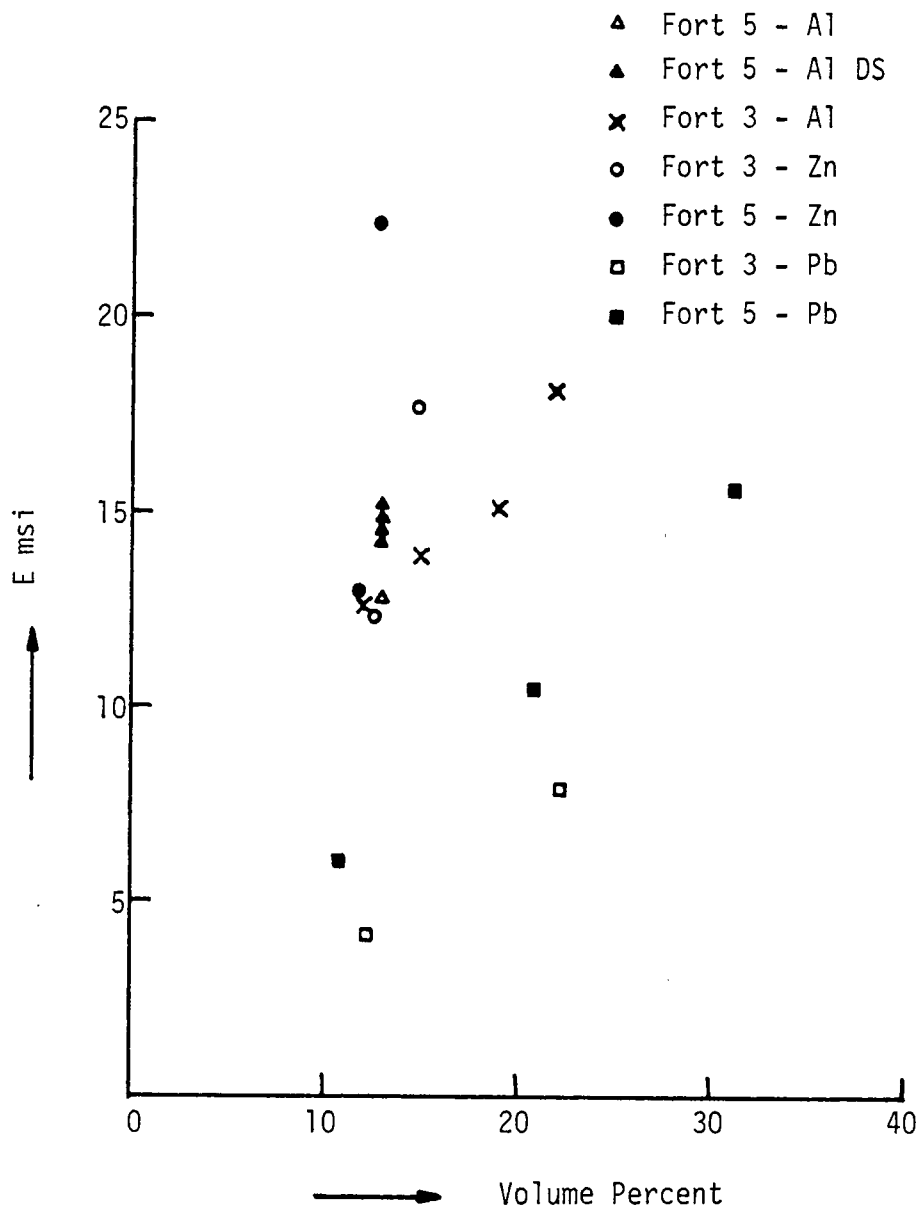


Figure 31. Tensile modulus vs. volume percent of fibers plot of various composites (as-cast and after-directional solidification in the case of Al - graphite).

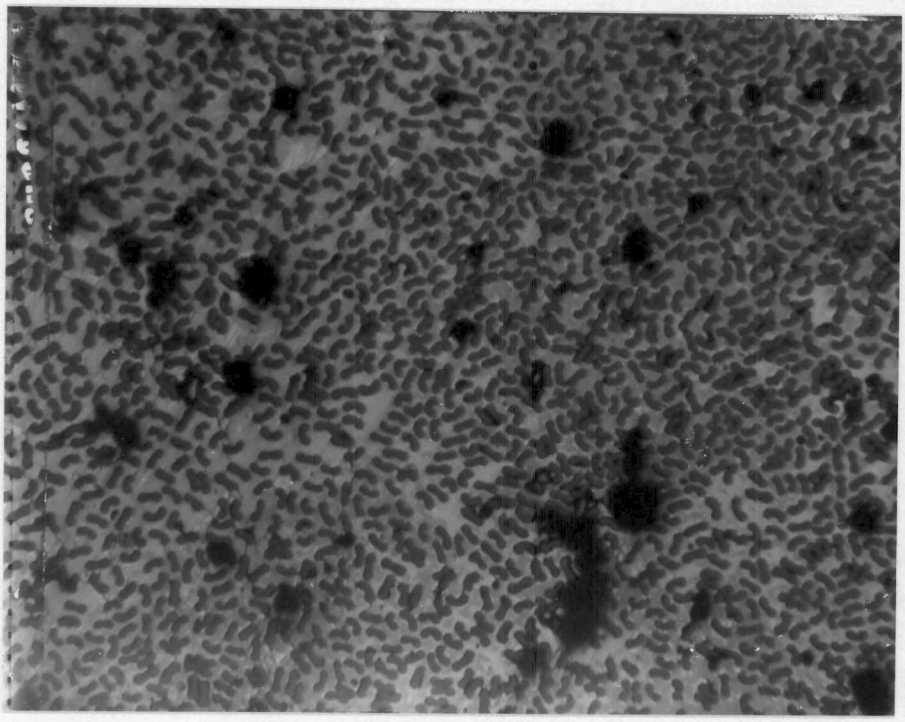


Figure 32. Transverse micrograph of Fortifil 5 and Fortifil 3 graphite fiber composites.

Transverse micrograph of Fortifil 5 graphite fibers-7075-Al alloy composite in as-cast condition, 200X.

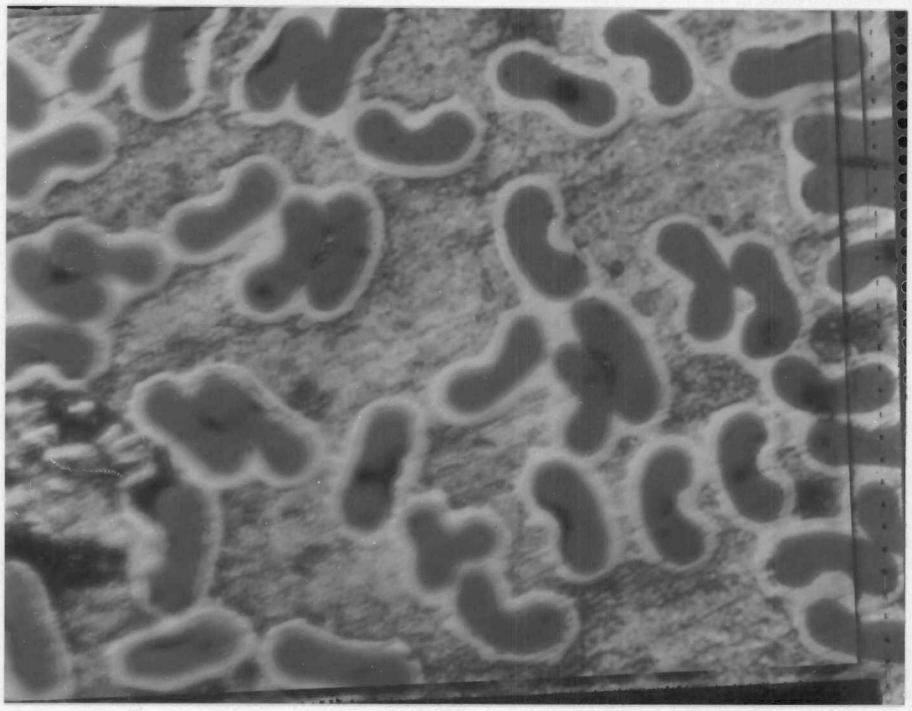


Figure 32. (Continued)

Transverse micrograph of Fortifil 5 graphite fibers-Pb composite (11v/o-fibers), 1210X.

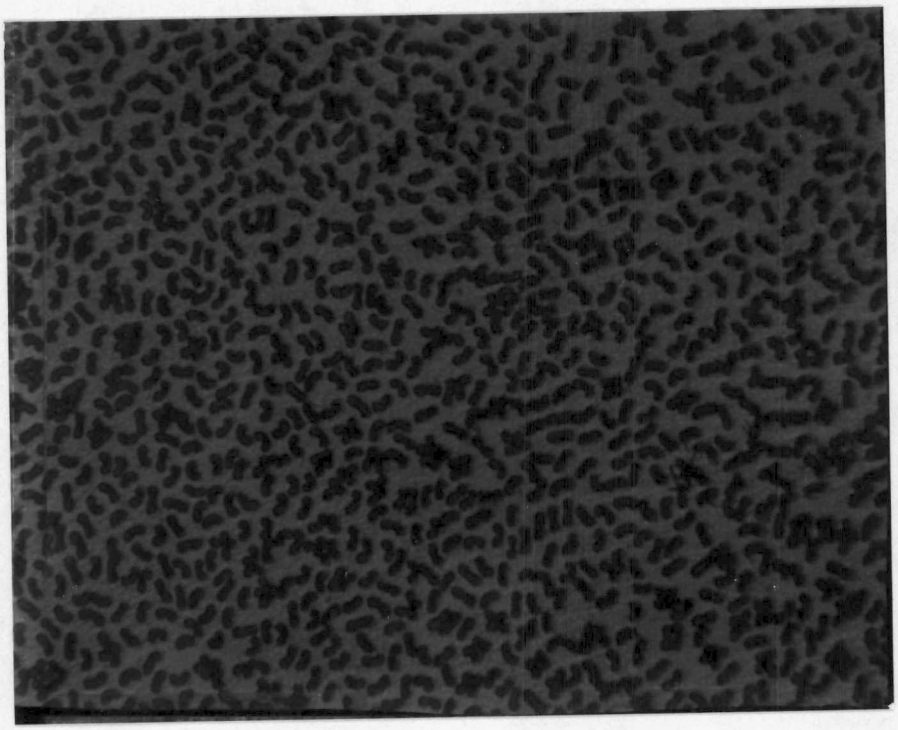


Figure 32. (Continued)

Transverse micrograph of 18v/o Fortifil 3 graphite fibers-Zn composite, 300X.

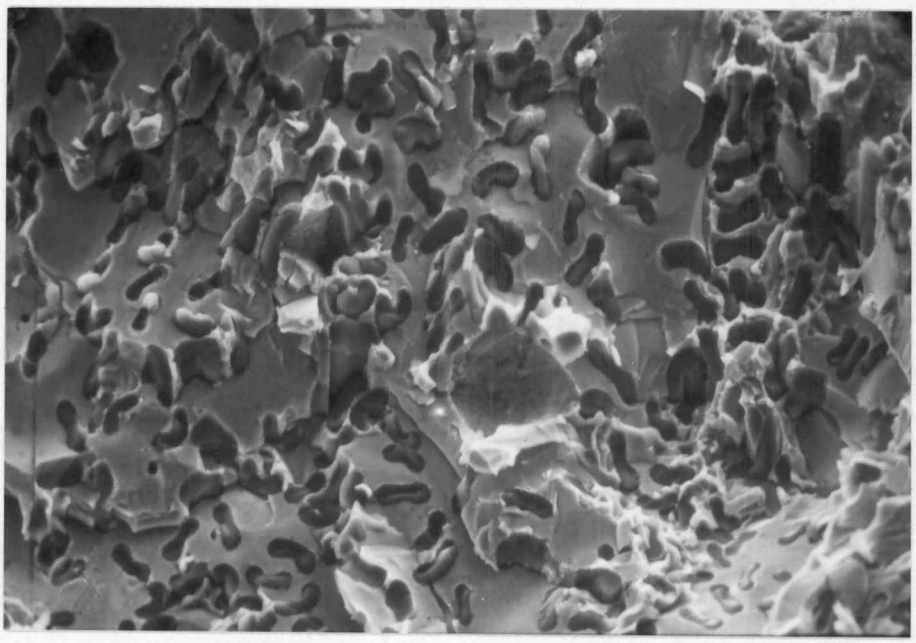


Figure 33. SEM photograph of the fractured surface of Fortifil 5-7075Al composite (as-cast), 400X.

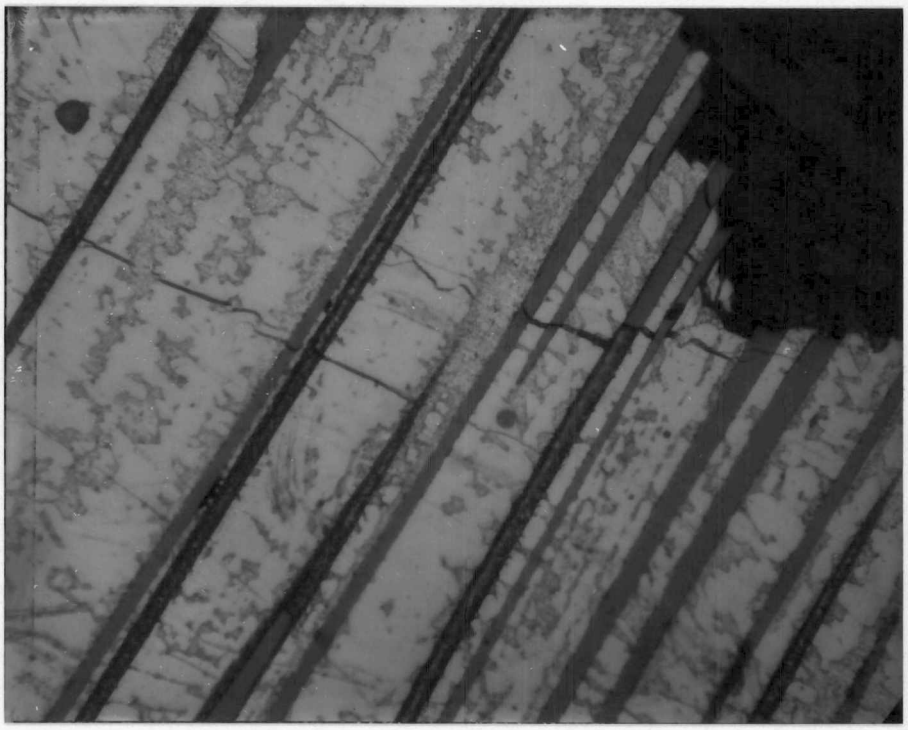


Figure 34. The crack propagation through brittle Al_3Ni matrix in as-cast Fortifil 5-7075Al composite, 236X.

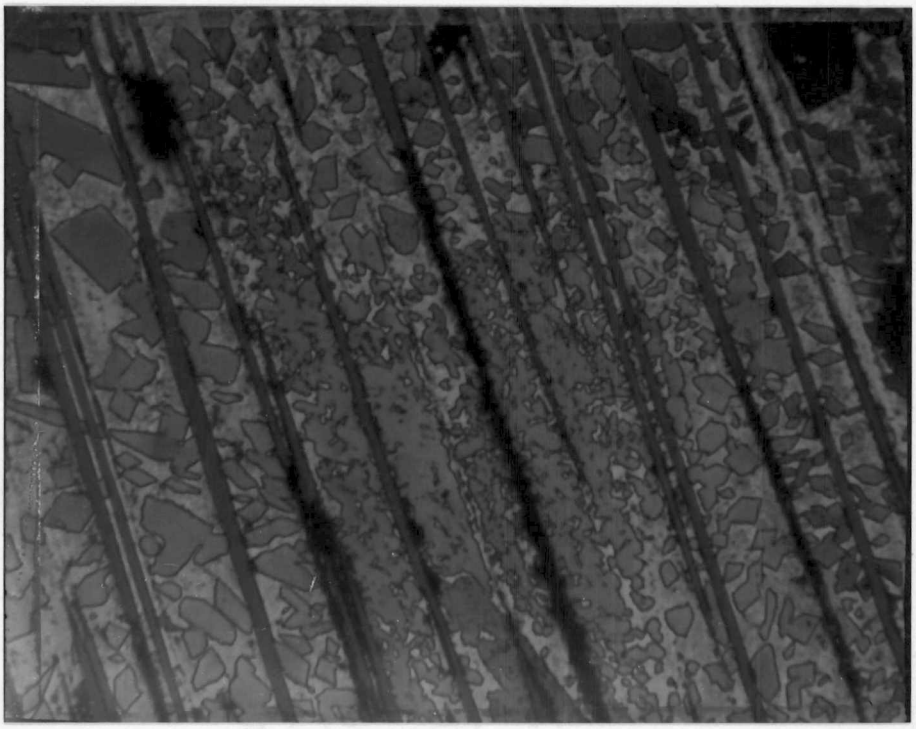


Figure 35. Longitudinal micrographs of Fortifil 5-7075Al composites. Longitudinal micrograph of as-cast Fortifil 5-7075Al composite, 236X.



Figure 35. (Continued)

Longitudinal micrograph of the middle of the Fortifil 5-7075Al composite specimen after passing the zone (10"/hour), 236X.



Figure 35. (Continued)

Longitudinal micrograph of the end of the Fortifil 5-7075Al composite specimen after passing the zone (10"/hour), 236X.

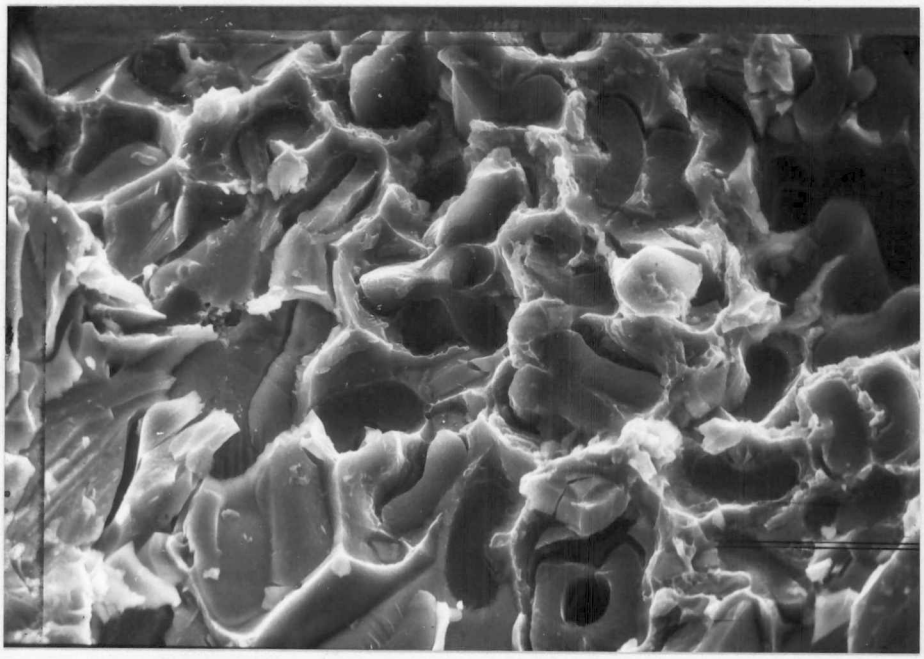


Figure 36. SEM photograph of fractured surface of Fortifil 5-7075Al composite directionally solidified at 10"/hour rate, 1000X.

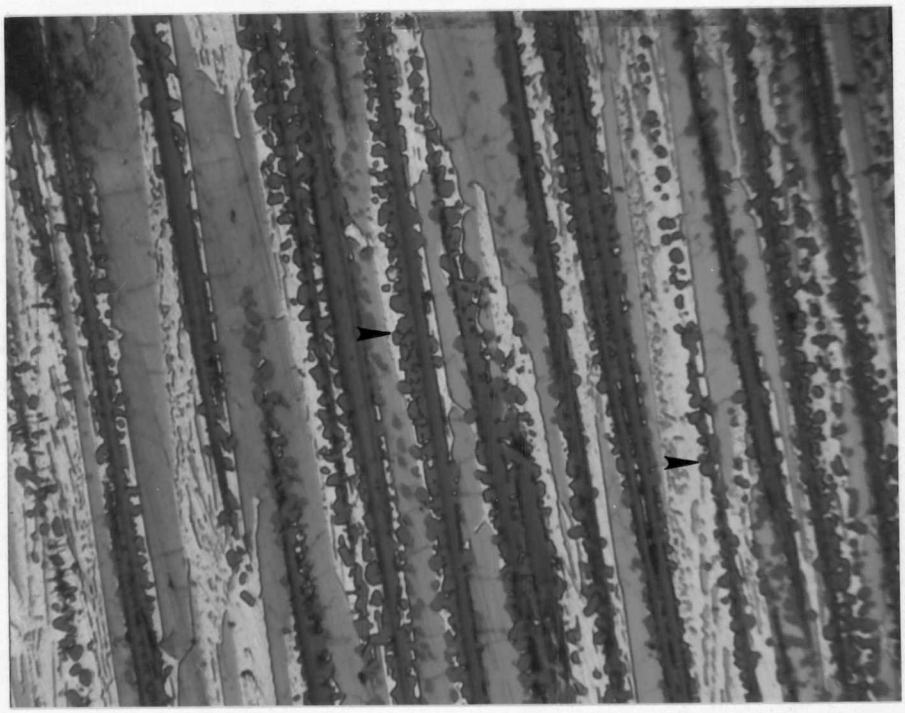


Figure 37. Longitudinal micrograph of the directionally solidified Fortifil 5-7075Al composite. The solidification rate being 2.5 inches per hour, 236X.

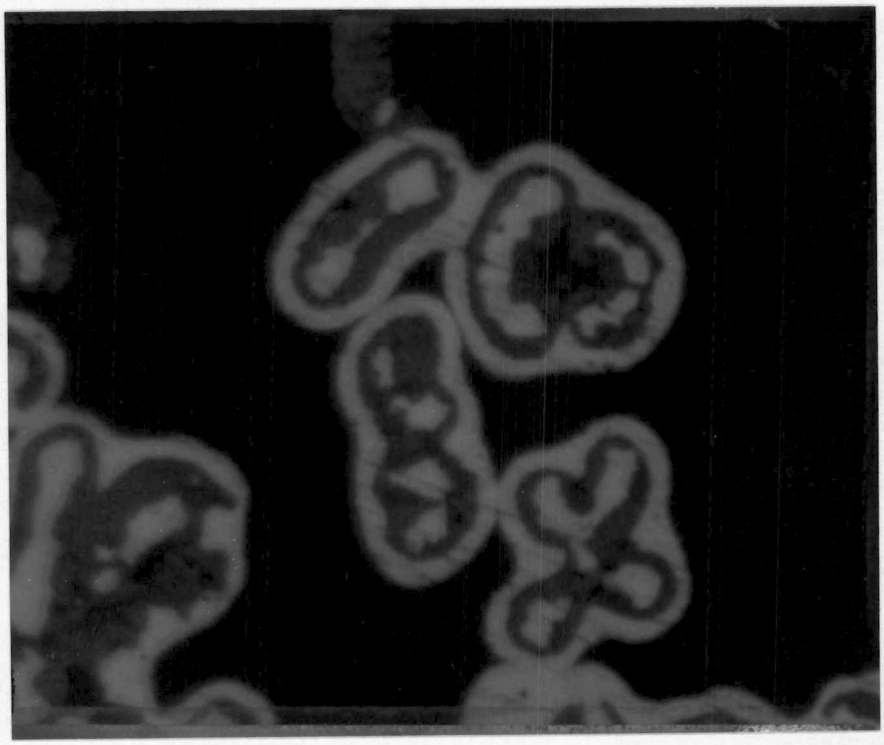


Figure 38. Fortifil 5 graphite fibers Ni-coated, heated at 1,100° C for one hour and again Ni-coated and heat-treated at 1,100° C for one hour in vacuum, 1815X.

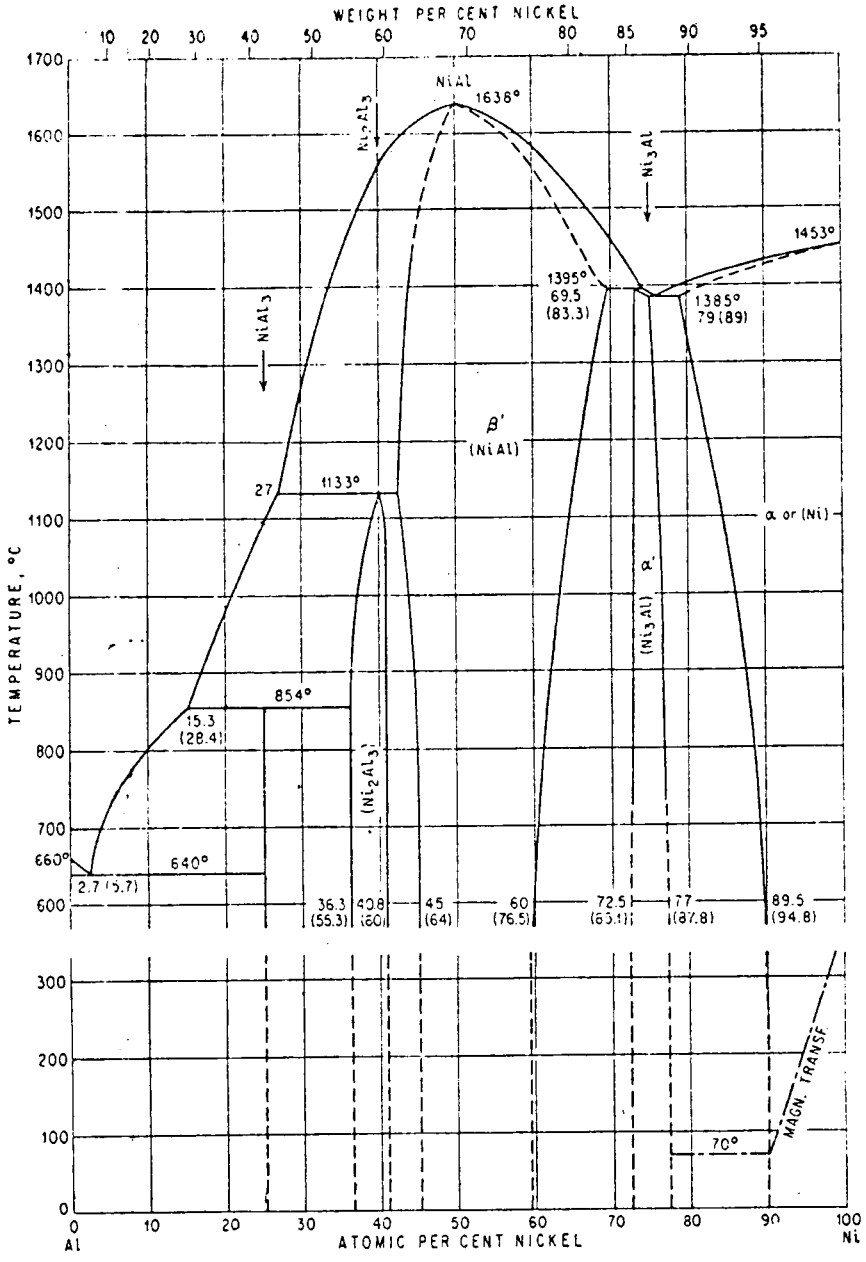


Figure 39. Al-Ni equilibrium diagram.

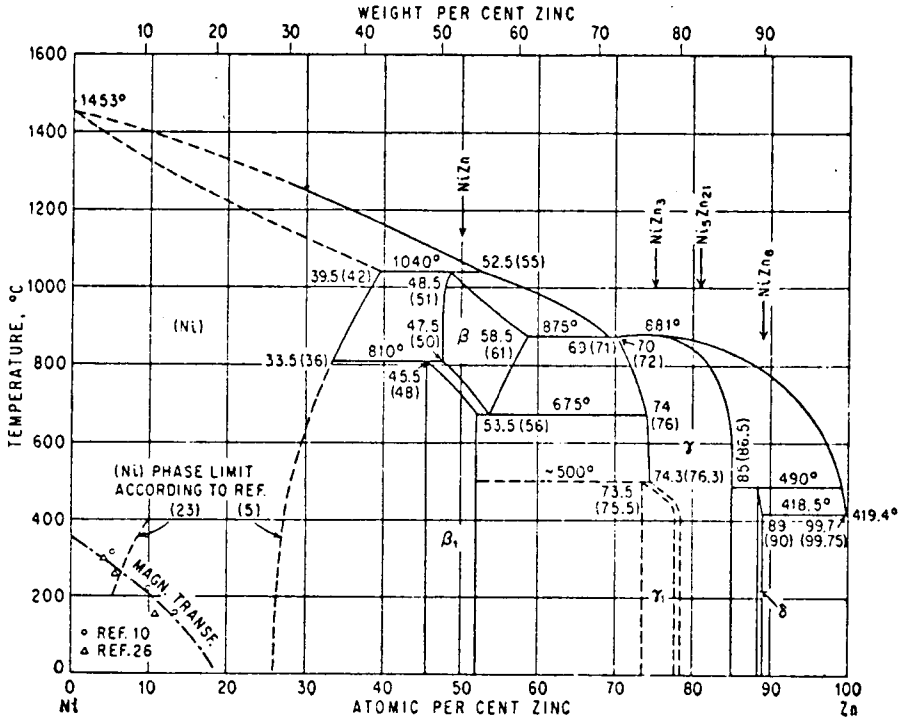


Figure 40. Ni-Zn equilibrium diagram.

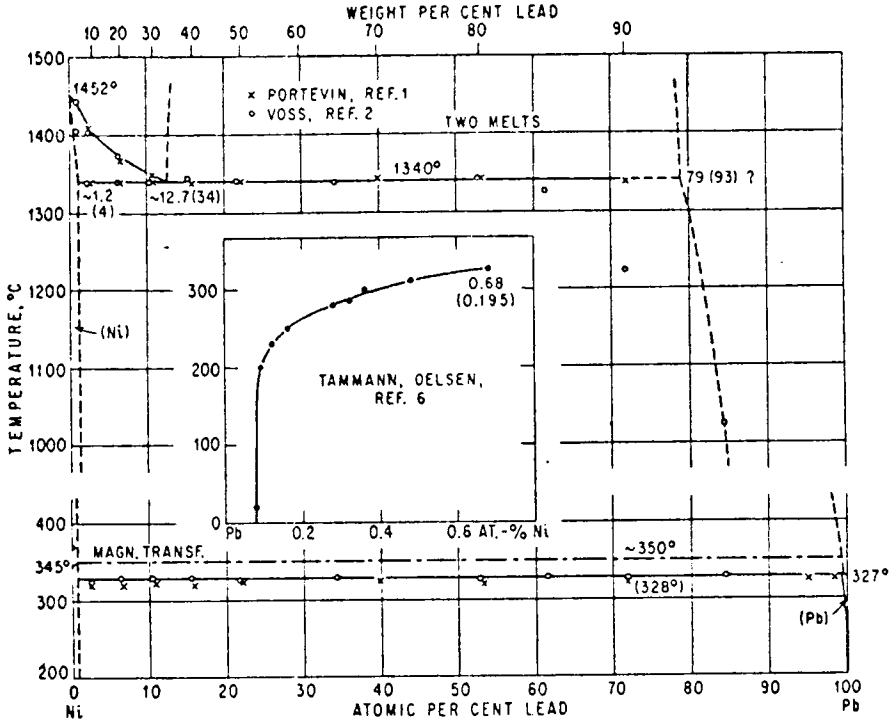


Figure 41. Ni-Pb equilibrium diagram.

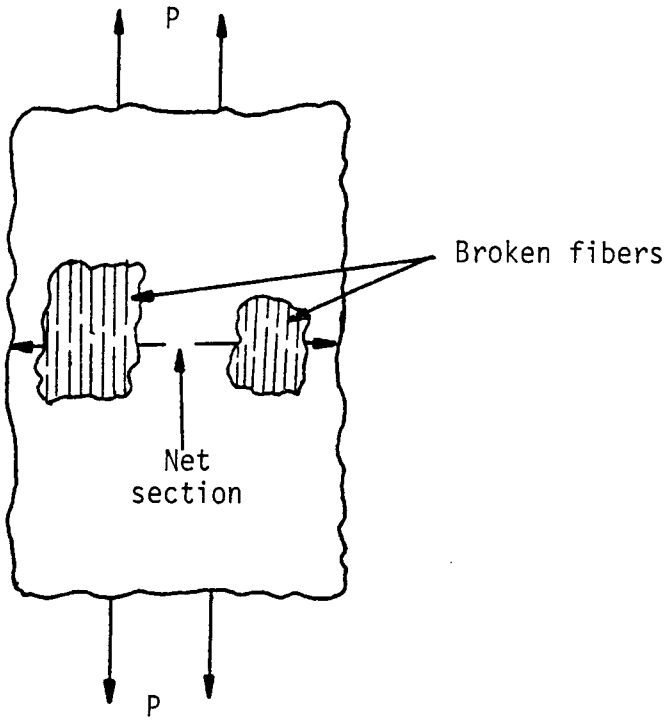


Figure 42. Model of local high-void density volume of bundle fracture.

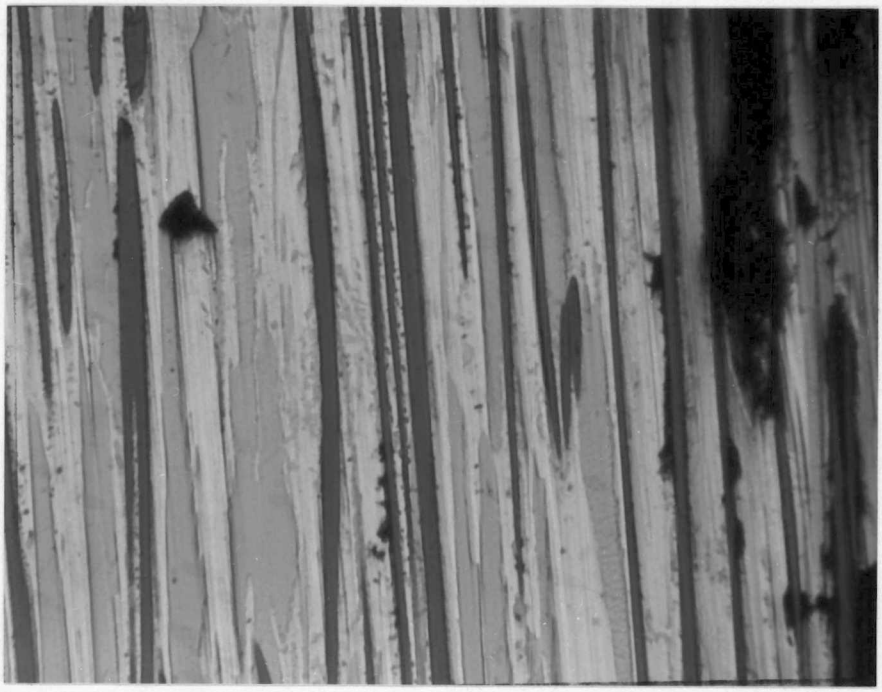


Figure 43. Longitudinal micrograph of Fortifil 5 graphite fibers-7075Al composite after directional solidification. Rate of zone passing 14"/hour, 236X.

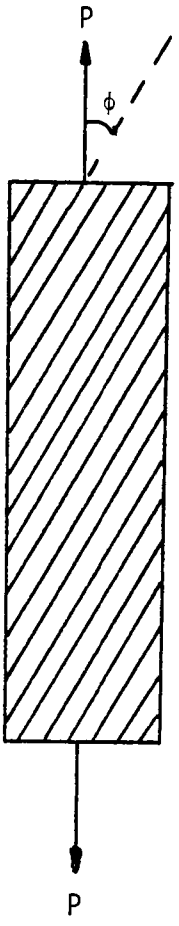


Figure 44. Fiber orientation. Schematic representation of a composite containing aligned fibers oriented at an angle ϕ to the tensile axis.

VITA

Raj K. Kaul was born in Srinagar, Kashmir, India, on March 27, 1950. In 1970, he received a Bachelor of Science degree in Physics, Chemistry, and Math at Punjab University. In 1974, he received a Bachelor of Science degree in Metallurgical Engineering from Punjab Engineering College. In 1977, Mr. Kaul received a Master of Technology degree in Metallurgical Engineering from Indian Institute of Technology in Kanpur.

In September 1977, he entered The University of Tennessee Space Institute Graduate School located in Tullahoma, Tennessee, which is a campus of The University of Tennessee, Knoxville. He received his Doctor of Philosophy degree with a major in Engineering Science in August 1984.

The author is a member of The Metallurgical Society--American Institute of Metallurgical Engineers (TMS-AIME). Mr. Kaul will be employed with The University of Tennessee Space Institute in the Materials Division after graduation.